Microstructure and Mechanical Properties of Titanium-Copper Reinforced Alumina Composites

Endale Chalew

A Thesis Submitted to
The department of Material Science and Engineering

School of Mechanical, Chemical and Materials Engineering
Presented in Partial Fulfillment of the Requirement for the Degree of Master's in Materials Science and Engineering

Office of Graduate Studies
Adama Science and Technology University

Adama
June, 2018

Microstructure and Mechanical Properties of Titanium-Copper Reinforced Alumina Composites

Endale Chalew

Ass. Prof. JeongKyun Kim

Prof. H. C. Ananda Murthy

A Thesis Submitted to

The department of Material Science and Engineering

School of Mechanical, Chemical and Materials Engineering

Presented in Partial Fulfillment of the Requirement for the Degree of Master's in Material Science and Engineering

Office of Graduate Studies

Adama Science and Technology University

Adama

June, 2018

Supervisor's/Advisor's approval sheet

To: ..... department

Subject: Thesis Submission

This is to certify that the thesis entitled "----------

----------submitted in partial fulfillment of the requirements for the degree of Master's in ----------, the Graduate program of the department of ----------, and has been carried out by ---------- Id. No ----------, under my supervision. Therefore, I recommend that the student has fulfilled the requirements and hence hereby he can submit the thesis to the department.

_____ _____ _____

Name of major Advisor/supervisor Signature Date

Declaration

I hereby declare that this MSc Thesis is my original work and has not been presented for a degree in any other university, and all sources of material used for this thesis/ dissertation have been duly acknowledged.

Name: _____

Signature _____

This MSc Thesis has been submitted for examination with my approval as thesis advisor.

Name: _____

Signature: _____

Date of submission _____

ACKNOWLEDGEMENT

Firstly, I would like to express my sincere gratitude to my advisor Prof. Jeongkyun Kim For the continuous support of my related research, for his patience, motivation, and immense knowledge. His guidance and his hard questions incented me to widen my research from various perspectives and helped me in all the time of research and writing of this thesis. Furthermore I would like to thank my co-advisor Prof. H. C. Ananda Murthy for his interest in my work and non-stop guidance and follow up. I could not have imagined having a better advisors and mentor for my M.Sc. study.

Besides my advisor, I am very thankful for the department chairs', Dr. Dinsefa Mensur, appreciation, guidance and support on the project and his encouragement throughout my study.

I would like to thank my friends who were not just a friend but also a colleague, for their insightful comments and encouragement, and also for their support in the experimental works. A special appreciation also goes to Eden Kebede for supporting me to finish the thesis on time by giving a warm motivation and taking part in writing it.

My sincere thanks also goes to Addis Ababa institute of technology, department of chemical engineering technical assistants and staffs who provided me access to their laboratory and research facilities. Without their precious support it would not be possible to conduct this research.

Last but not the least, I would like to thank my family: my parents and to my brothers and sister for supporting me spiritually throughout writing this thesis and my life in general.

List of Acronyms and Abbreviations

CMC: Ceramic matrix metal composite

XRD: X-ray diffractometer

PMC: Polymer matrix composites

MMC: Metal matrix composites

CAMS: Carbon matrix composites

CCC: Carbon-carbon composites

IPN: In interpenetrating network

IUPAC: International Union of Pure and Applied Chemistry

PFA: Pore forming agents

PVC: Polyvinyl chloride

PS: Polystyrene

PVB: Polyvinyl butyral

PMMA: Polymethylmethacrylate

PFA: Pulverized fuel ash

CVD: chemical vapor deposition

TEM: Transmission electron microscope

LEFM: Linear elastic fracture mechanics

CTE: Coefficient of thermal expansion

SHS: Self-propagating high temperature synthesis

IF: Indentation fracture

PLS: Pressureless sintering

DCM: Direct crack measurement

GNS: Graphene nanosheet

COD: Crack opening displacement

ASTM: American society for Testing and Materials

HFIHS: High-frequency induction heat sintering

CONTENTS

CHAPTER PAGE

LIST OF TABLES

TABLE **PAGE**

LIST OF FIGURES

FIGURE **PAGE**

Abstract

Al_2O_3 is considered as a valuable industrial material and the most widely used ceramic. It possesses good mechanical properties however, its applications as a structural material have been limited by it low fracture toughness and low-fracture strength. This is because cracks easily propagate in this ceramics and therefore they might fail unpredictably in service. The main objective of this work was demonstrating the effect of reinforcing Ti and Cu metallic particles in to Al_2O_3 to overcome its limitations on the above application areas and improve its mechanical properties. The synthesis of Al_2O_3-based composites having different amount of fine titanium and copper reinforcement particles was investigated and Ti and Cu metallic particles were reinforced to Al_2O_3 with different compositions. The powders were first prepared with the appropriate stoichiometric ratio, milled in order to create a homogeneous distribution of particles and reduction of size, the milled powder was then compacted to form a green body which is finally sintered at 1100^oC, 1200^oC and 1300^oC for 2 and 3 hours for a better densification and reduction of porosity. For the samples with 3%Ti-3%Cu and 3%Ti-2%Cu the controlled grain growth and the homogeneous distribution of Ti and Cu along with the better wettability of Cu with Ti accentuate the obtainment of dense bodies with homogeneous microstructures, which leds to a better density and fracture toughness as well as better electrical resistance. Therefore, this study proves that a controlled reinforcement of Ti and Cu can significantly improves the mechanical properties of Al_2O_3, specifically the fracture toughness.

CHAPTER 1 INTRODUCTION

1.1 General introduction

Ceramics, in general, are characterized by high stiffness and hardness; resistance to wear, corrosion, and oxidation; and high-temperature operational capability. However, they also have serious deficiencies which have severely limited their use in applications that are subjected to significant tensile stresses. Ceramics have very low fracture toughnesses, which makes them very sensitive to the presence of small flaws. This results in great strength scatter and poor resistance to thermal and mechanical shock.

Alumina is a very useful industrial material and the most widely used oxide ceramic. [1–3] Its applications span from high-speed cutting tools, dental implants and prostheses, electrical and thermal insulators, wear resistant parts, and coatings. Its usefulness is attributed to its high hardness, inertness, high compressive strength, and high electrical and thermal insulating properties. However, despite its enviable properties and potentials, its use as a structural material has been considerably hindered by its low-fracture strength and low-fracture toughness (as is typical of ceramics). [4–7] Cracks readily propagate in ceramics; thus, they fail unexpectedly in service, and in most cases, catastrophically, during impact even when the impact load is below the strength of the ceramic material. Resistance to crack growth lies in the ability to activate a toughening mechanism such as crack bridging, crack deflection, or transformation toughening, among others. The mechanical properties of ceramics are known to be improved significantly by dispersing nanometer-sized ceramic particles into the ceramic-matrix grains or grain boundaries, and there are several mechanisms to achieve better mechanical properties. The mechanisms include transformation toughening, toughening by a metallic particulate phase, and fiber reinforcement. In this study, toughening by a metallic phase will be discussed briefly, which is also called Cermet. Any macroscopic crack which occurs in the material leaves behind metal particles, or ligaments, which bridge the crack surface just behind the crack tip restraining its opening. For this mechanism to be effective it is essential that the particles be well-bonded to the matrix and that the advancing crack tip be drawn to particles so that bridges are left behind.

Ceramic-metal composites are an exciting field of research, enabling a combination of properties not possible in monolithic metals or ceramics.

The four primary categories of composites are polymer matrix composites (PMCs), metal matrix composites (MMCs), ceramic matrix composites (CMCs), and carbon matrix composites (CAMCs). Carbon–carbon composites (CCCs) are the most important subclass of CAMCs. At this time, PMCs are by far the most widely used type of composites. [8]

In this study, Al_2O_3 will be reinforced with Ti and Cu particles through the dry ceramic processing technique. The effect of Ti and Cu particulates on the microstructure of Al_2O_3 matrix will be investigated. Moreover, the mechanical properties of composite materials will be examined via Vicker's microhardness test and finally, microstructure observations will be made with optical microscopy and scanning electron microscopy. Photographic evidence of arrest of crack growth by metallic particles will be obtained, demonstrating that the reinforcement mechanism of these materials is due to the deflection of cracks owing to metallic bridges formed by the metal used as alumina strengthener.

1.2 Statement of the problem

Alumina (Al_2O_3) exhibits favorable physical and chemical properties such as; high strength, hardness, elastic modulus and excellent resistance to thermal and chemical environments. However, its applications are somewhat limited because of poor toughness and inferior thermal shock resistance and most structural Al_2O_3-based ceramics present poor electrical conductivity.

1.3 Objectives of the Study

1.3.1 General Objective

The general objective of this work is to investigate the effect of the addition of Ti and Cu on the mechanical properties of Al_2O_3.

1.3.2. Specific Objectives

The specific objectives are as follows:

- ✓ Synthesis of ceramic matrix metal (CMC) composites.
- ✓ Mechanical property, specifically fracture toughness evaluation of Ti-Cu reinforced Al_2O_3.
- ✓ Studying the mechanisms for the improvement of mechanical properties and performance of Alumina.
- ✓ Investigating the combined properties gained through using two different metallic particles as a reinforcement to Alumina ceramics.

1.4 Scope of the Study

The scope of this thesis work focuses on the microstructure and the mechanical properties, particularly fracture toughness, of Ti-Cu reinforced Al2O3 composite. The study includes both synthesis (by dry ceramic processing technique) and characterization (using optical microscope, Vickers microhardness tester, and XRD). The value of fracture toughness will be determined from the experimentally obtained hardness and crack size results.

1.5 Significance of the study

The findings of this study will be an initial input for students and researchers who are interested in this area and encourage professionals to carry out such kind of researches in the field for the benefit of the scientific world considering that materials science and engineering plays an important role in science and technologies today. Other attributes of the proposed project includes: It contributes an alternative method to the scientific world. For the researcher, to uncover critical areas in researching. Thus, a new approaches on synthesizing ceramic-metal composites may be arrived at, and enhance what he has grasp theoretical and practical knowledge during the study. It will be a very good reference for further study on microstructure and mechanical properties of ceramic-metal composites.

CHAPTER 2 LITERATURE REVIEW

2.1. Composite Materials

Composites are multifunctional materials having unprecedented mechanical and physical properties which can be tailored to meet the requirements of a particular application. Many composites also exhibit great resistance to wear, corrosion, and high-temperature exposure. Composites technology also makes possible the use of an entire class of solid materials, ceramics, in applications for which monolithic versions are unsuited because of their great strength scatter and poor resistance to mechanical and thermal shock. Composites are usually classified by the type of material used for the matrix. The four primary categories of composites are polymer matrix composites (PMCs), metal matrix composites (MMCs), ceramic matrix composites (CMCs), and carbon matrix composites (CAMCs). Carbon–carbon composites (CCCs) are the most important subclass of CAMCs. At this time, PMCs are by far the most widely used type of composites. [8] CMCs tend to have particularly good resistance to corrosion, oxidation, and wear, along with high-temperature capability. Monolithic ceramics are brittle materials with very low fracture toughness, because of which their strengths display great scatter. As a result, they are not useful materials for applications that are subjected to significant tension or torsional stress. Therefore, it needs to reinforce them with metallic particles for a better mechanical properties and enhanced toughness. The key ceramics used as CMC matrices are silicon carbide, alumina, silicon nitride, mullite, and various cements. The properties of ceramics, especially strength, are even more process sensitive than those of metals. In practice, it is very difficult to determine the in situ properties of ceramic matrix materials in a composite.

2.2. Production of ceramic-metal composites

There are three types of ceramic-metal composites. Metal Matrix Composites (MMC) have a continuous metal network, typically with $V_{metal} > V_{ceramic}$. Ceramic Matrix Composites (CMC) have a continuous ceramic network, usually with $V_{ceramic} > V_{metal}$, although there are exceptions. In interpenetrating network (IPN) composites both components are continuous. The only limitation on composition is that there is enough of each phase for both to percolate. Depending on the form, for the minority phase this is around 20 to 30 %, less for fibres and more for particles. The advantages of an IPN include a higher Young's modulus,

hardness and load bearing capacity than MMCs, as well as a higher thermal conductivity and higher fracture toughness than CMCs. In the naming of such composites, either the matrix phase for MMCs and CMCs or the majority phase in IPN is mentioned first.

2.2.1. The porous ceramic preform

To produce an IPN ceramic-metal composite, the first step is to produce a macroporous ceramic preform. Macroporous is defined by IUPAC recommendations as exhibiting a pore width/diameter > 50 nm [9]. There is a variety of methods for producing open porous ceramics described in the literature, ranging from patents in 1963 [10] to current reviews [11, 12], allowing the tailoring of the microstructure. The porosity and pore sizes reported vary between 20 and 97 % and 400 nm to 4 mm, respectively [11]. The different methods available have been summarized in figure 2.1. These methods can be grouped into four categories: i) partially sintered, ii) sacrificial template, iii) replica and iv) foaming and setting. The ranges of porosities and grain sizes reported for each category are shown in figure 2.1. Each of the four categories are described briefly below and shown schematically in figure 2. For this project, ceramics with pore sizes from 1 to 30 μm and open porosities of 20 to 60 % are required. For this reason the first two categories will be considered in more detail later. A recent review by Studart et al. [11] provides a comprehensive summary of these methods. Many references for each particular method are also included in this review.

i) Partially sintered: Partial sintering involves either dry pressing or slip casting and drying and then firing. Porosities up to 40 % are achievable [15].

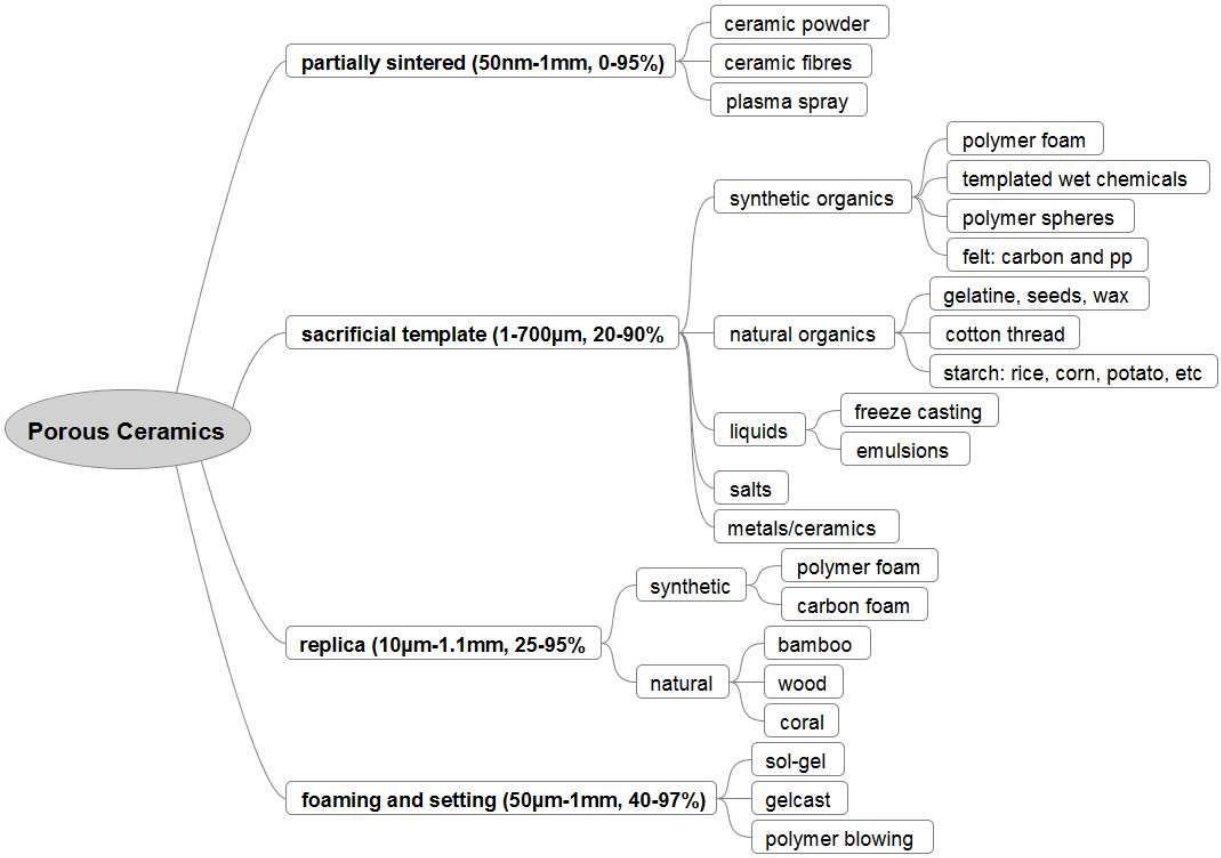

Figure 2.1: Overview of methods for producing porous ceramics [11,13,14].

The pores are homogeneously distributed within the microstructure [16]. Plasma spraying involves the spraying of molten or heat-softened material onto a surface to provide a coating. Ceramic powder is injected into a plasma flame, where it is rapidly heated and accelerated to a high velocity. The hot powder impacts on the substrate surface and rapidly cools forming a coating. A porosity of 15 % was reported by Travitsky et al. [17]

ii) Sacrificial template: The sacrificial material is added to the ceramic precursor (powder or slurry) then dried. The sacrificial material is then removed, either by pyrolisation, melting, evaporation or leeching. Finally the ceramic is sintered. This results in a porous ceramic body with a negative replica of the original sacrificial template. A wide variety of templates including network structures, pyrolysable particles, liquids, salts, metals and ceramics have been reported [11]. This wide range available provides flexibility in the ranges of achievable porosity and pore size, with 20 to 90 vol.% and 1 μm to 1 mm, respectively, being reported in the literature [11].

iii) Replica: The replica template material has a solid network structure, for example foam or wood. The template is infiltrated with a ceramic slip. Excess slurry is removed leaving a ceramic coating on the template, which is then dried. Upon heating, the template is pyrolysed and the ceramic coating sintered. This results in a 25 to 95 vol% porous ceramic body with pore sizes ranging from 10 to 130 μm for wood and 100 μm to 1.1 mm for polymer foam [11]. The microstructure is a positive replica of the template, but with hollow struts. With a polymer foam replica, the triangular strut profile causes stress concentration at the corners and has been found to cause strut cracking and therefore lower strength [18, 19]. Wood has a radial structure and can contain knots and other irregularities [20].

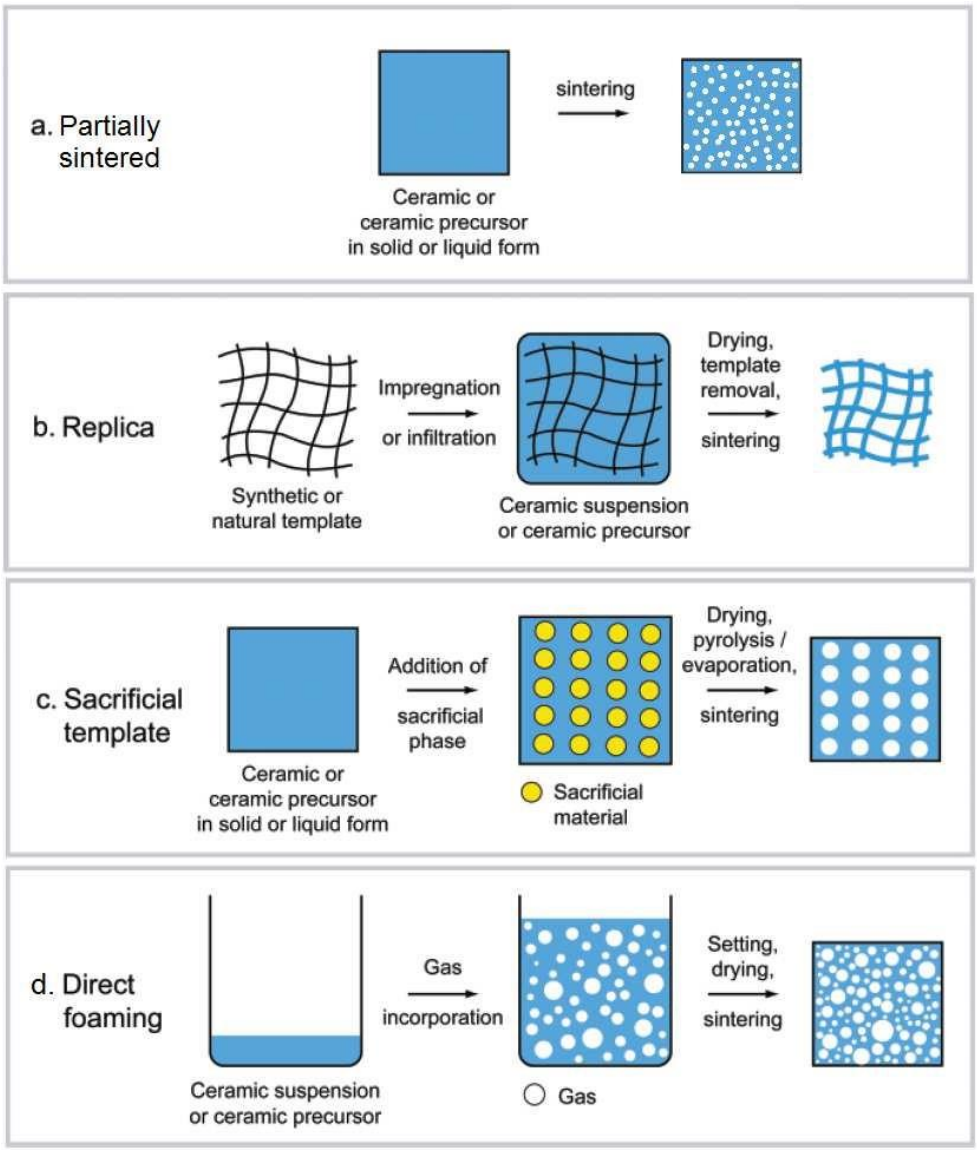

Figure 2.2: Processing routes for the production of porous ceramics [11].

iv) Foaming and setting: In this process gas is incorporated into a ceramic slip to form bubbles. A surfactant is used to stabilise the resulting ceramic foam. The foam is allowed to set and dry before sintering. There are numerous methods of incorporating the gas and stabilizing the ceramic foam, as described in reviews by Studart et al. [11] and Saggio-Woyanski et al. [13]. The resulting porosity can be either closed or open, depending on the stability of the foam. The achievable pore sizes are 50 μm to 1 mm.

Table 2.1: Largest pore space and entrance diameter of monomodal sphere packing relative to sphere size [21].

	Loosest packing	most dense packing
Entrance diameter	0.414	0.155
Largest pore space	0.732	0.414

Partial sintering

Partial sintering of a pressed ceramic powder or dried ceramic slip results in a homogeneous pore distribution and pore size [16]. A ceramic slip can be cast, which results in a homogeneous density in the cast part. Using a compacted ceramic powder allows higher porosities to be achieved, but one is limited to a simple shape and it is more difficult to achieve homogeneity in the packing of the powder. When the powder is pressed, it has been observed that the shape of alumina grains are irregular and deviate from a spherical shape [21]. For a monomodal ceramic powder, the largest pore space and entrance diameter (smallest pore space) can be calculated as a function of grain size and packing density [22]. The factors for the highest and lowest packing densities are given in table 2.1. To obtain an entrance diameter of 1 μm, a ceramic powder with a grain size between 2.4 and 6.5 μm is required, depending on the packing density. For example, to achieve the target channel size of 1 μm, Skirl et al. used a ceramic powder with an average grain size of 5 μm [23].

Polymer foam and felt

The polymer foam (sacrificial template) method was developed by Lange et al. [14]. Schwarzwalder and Somers patented a similar method earlier in 1963 [10]. However, this replica method included a step of excess slurry removal resulting in high porosities from 50 to 95 %. In the method by Lange et al., polymer foam is infiltrated with a ceramic slip using pressure filtration, dried, and then pyrolysed to give a porous ceramic with a negative replica of the foam. The ceramic green body is then fully sintered. In this method the porosity of the ceramic body was limited by the density of the polymer foam: 2.5 % for low density foam and 15 % for high density foam. In order to achieve higher densities, the foam can be compression moulded before slurry infiltration [24–26]. The foam is typically compressed in one direction to give the desired porosity, typically to an eighth or tenth of the original thickness. An anisotropic structure is thus formed.

The structure of the porous ceramic formed in this method (figure 2.3) has a notable disadvantage [26]; the corners of the triangular pore channel cross section act as stress concentration points. During the stages of drying and sintering the ceramic shrinks. This leads to microcracking of the ceramic, typically at the stress concentration points, which in turn causes a decrease in the strength and elastic modulus of the composite.

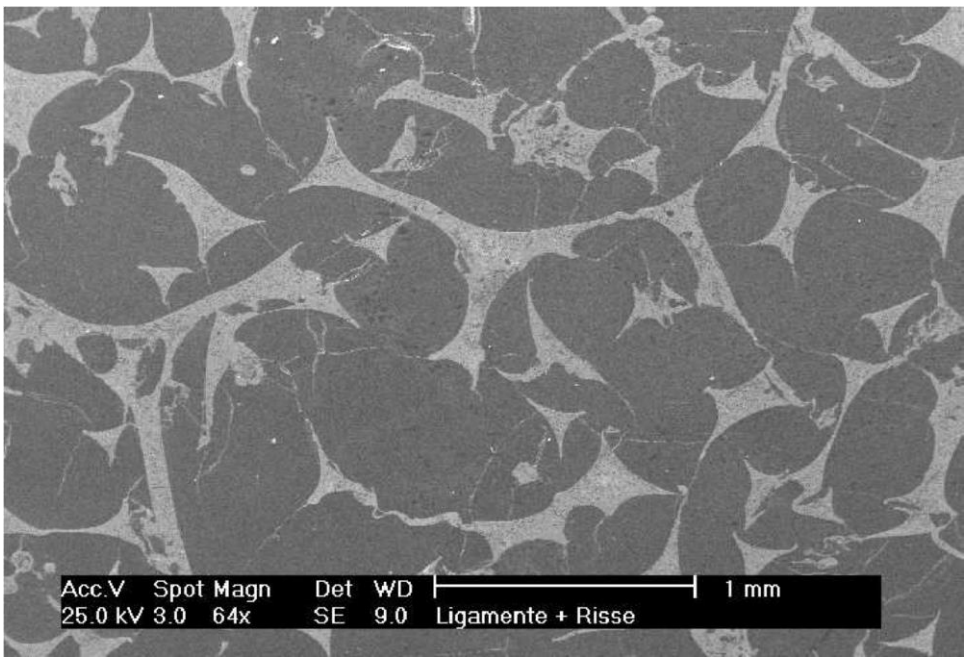

Figure 2.3: Electron microscope image of a polymer foam based alumina-copper composite. Copper-filled cracks in the ceramic phase can be seen [27].

It would thus be desirable to have a pore structure with rounded, rather than triangular, ligaments. One possibility proposed by Lange et al. was to use felt as the sacrificial preform [14]. However, no results were given, since the paper had concentrated on polymer foam. No other literature has been found mentioning felt. The rounded fibres in felt may potentially overcome the limitations of polymer foams. A novel variation on this method incorporates pyrolysis of the polymer foam to form carbon foam before slip infiltration [28]. However, this energy intensive step adds to the overall cost of the porous ceramic without any obvious benefits.

Pore forming agents

The use of so-called pore forming agents (PFA) as a sacrificial preform is well established [11]. In this method, pyrolysable particles are mixed into the ceramic slip, which is then dried and fired to burn out the particles and sinter the ceramic. The porosity and pore size of the resulting ceramic can be controlled by the amount of particles added to the slip and the size of the particles, respectively. Porosities ranging from 20 to 80 % can be achieved. Other pore forming agents mentioned in the comprehensive review by Studart et al. include polymer beads (PVC, PS, PVB, PMMA), cellulose, gelatine, seeds, starch powders, oil emulsions, salts, metal powder and carbon fibres and flakes [11]. Salts and metal powder are removed by washing or leeching of the preform. This method can be combined with partial sintering to achieve a combination of macropores and micropores. Depending on the shape and distribution of the particles, at least 15 to 30 % PFA is required to achieve open porosity. Below this amount the porosity may be all or partly closed.

The main disadvantage of this process is that the ’windows’ connecting the pores are much smaller than the pores themselves. This bottleneck leads to a lower permeability than what would be expected for the given pore size, which in turn requires higher pressures for metal infiltration. Care must be taken to ensure the PFA particles stay homogeneously distributed in the ceramic slip during casting and drying in order to ensure a homogeneous pore structure. Starch absorbs water leading to swelling of the particles and a larger-than-expected pore size. This also reduces the bottleneck effect, since the soft, swollen particles do not remain perfectly spherical, but rather compress together at points of contact resulting

in larger pore windows. Mattern also reported clumps of alumina powder within the pores [29]. It is claimed to be due to the shrinkage of the starch particles during drying and pyrolisation. This was not observed with PMMA spheres, apparently since they neither wet the alumina slurry, nor do they shrink during the drying stage.

2.2.2. Metal infiltration

Due to the poor wettability of liquid copper on alumina (discussed further in section 2.1.3), pressure is required to infiltrate copper into the porous alumina preform. Widespread methods used include squeeze casting [14] and gas pressure infiltration [30]. Garcia-Cordovilla has written an extensive review on the subject [31].

a) Squeeze casting: The squeeze-cast method applied to porous ceramic preforms is described by Lange et al. [14]. Firstly, the porous ceramic preform and stainless steel die are preheated. The ceramic preform is then placed in the die. Molten metal in a separate crucible (100 to 150 K above the melting point) is poured over the ceramic. A hydraulic plunger then forces the molten metal into the pore channels of the ceramic preform at pressures around 100 to 200 MPa. The advantages of squeeze casting are that infiltration is carried out quickly, ceramic-metal reactions are thereby minimized, and a fine-grained microstructure without shrinkage voids can be achieved. The process is commonly used with alloys of aluminium, tin, zinc and silver. More recently, this method has also been applied to copper [32]. A disadvantage of this method is that some porous ceramics are not strong enough to withstand the high pressure applied, resulting in a crushed ceramic.
The ceramic preform must therefore be either strong or have a high permeability.

b) Gas pressure infiltration: Gas pressure infiltration of porous ceramics was first developed by Travitzky and Claussen [30]. The preform to be infiltrated is mechanically fixed to the bottom of an alumina crucible. The crucible is filled with pieces of plate metal and placed in a gas pressure furnace. The furnace is then heated above the melting point of the metal under vacuum to prevent oxidation of the metal. Pressure is applied by argon gas between 0.5 and 10 MPa forcing the metal into the pore channels of the ceramic preform. The system is then cooled below the melting point, continuing the application of pressure

until the metal has solidified. This method requires that the infiltrated ceramic be cut out of the solid metal filled crucible. Knechtel et al. applied this method to infiltration of copper into porous alumina [33]. The temperature and pressure of infiltration were 1350 °C and 15 MPa, respectively. Even at this pressure, pores of 0.08 μm could not be infiltrated. Prielipp et al. improved the process by securing the ceramic preform from above and incorporating a lift to raise and lower the crucible [34]. After infiltration the system is cooled to just above the melting point. While maintaining the high pressure, the crucible is lowered until the infiltrated ceramic is no longer in the molten metal. The system is further cooled until well below the melting point and the pressure then removed. In this way the infiltrated preform does not need to be cut out of the crucible. This method is quite slow in comparison to squeeze casting: one day compared to a few minutes [14].

c) Pressureless infiltration: If the wetting angle of the molten metal on the ceramic is below 90° the infiltration can be carried out without applied pressure, typically under vacuum. One major advantage of pressureless infiltration is that it is less expensive than the above two methods.

Alternative methods

A limited number of materials that exhibit spinodal decomposition can be used to created a composite in situ [15]. Commercial examples of this method include DIMOXTM and PRIMEXTM to produce alumina-aluminium composites. An alternative to molten metal infiltration is to fill the porous ceramic with metal via chemical vapour deposition (CVD) [15].

2.2.3. Ceramic-metal interface wetting

The wettability of a liquid on a solid substrate can be described by Young's equation [35]

$$\text{Cos}\,\theta = \frac{\gamma sv - \gamma sl}{\gamma lv} \tag{2.1}$$

Where γ_{lv}, γ_{sv}, and γ_{sl} represent the interface energies of liquid/vapour, solid/vapour and solid/liquid, respectively, and θ is the contact angle between the liquid drop and the solid substrate, as depicted in figure 2.4. If the contact angle is less that 90° the liquid is 'wetting', if greater than 90° it is 'non-wetting'. From equation 2.1 it is clear that a reduction in θ will result from increase in γ_{lv} or γ_{sl}, or a decrease in γ_{sv}.

Wetting can be classified as physical or chemical, depending on the nature of the bonding at the interface [36]. Physical wetting is due to reversible physical forces across the interface, such as Van der Waals forces or electrostatic attraction. In this case Young's equation can be used. The interface energy, γ, can, however, be influenced by adsorption of vapour at the solid-vapour interface [35] as described by equation 2.2:

$$\frac{d\gamma}{dlna} = -\Gamma RT \tag{2.2}$$

where a is the activity of the gas, which for an ideal gas can be replaced with pressure, Γ is specific adsorption, R is the universal gas constant and T is temperature.

Chemical wetting refers to chemical bonding across the interface. A reaction layer may form where both phases are in contact with the reaction layer rather than each other [37]. Young's equation is thus inadequate and must be modified. Aksay et al [38] proposed that the specific free energy of the reaction, Δg, be added to the solid-liquid interface energy, such that a negative Δg (required for spontaneous reaction) results in the lowering of γ_{sl}:

$$\gamma_{sl} = \gamma^{o}_{sl} + \Delta g \tag{2.3}$$

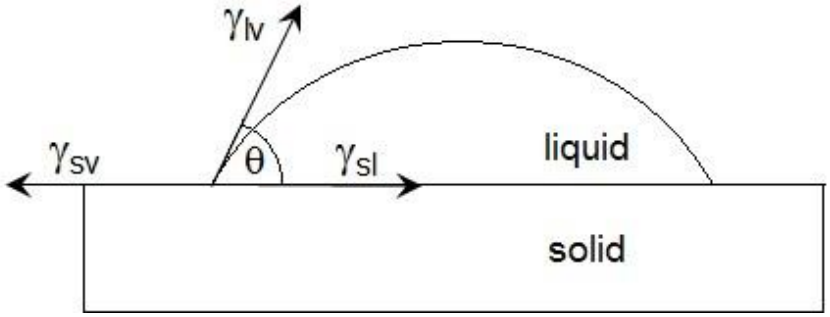

Figure 2.4: Schematic illustration of wetting.

where γ_{sl}^{o} is the initial or pure interfacial tension. It has been found that the equilibrium contact angle has the same value as the contact angle between the pure liquid metal and the reaction product layer, showing that the liquid metal wets the reaction product rather than the ceramic substrate [39].

The aforementioned equations all describe wetting and adhesion on a simple, flat surface. In order to consider curved surfaces such as pores or pore channels, pressure must be taken into account. The Laplace equation [35] shows that for a capillary with radius r_c, where the liquid forms a meniscus of radius R, the difference in pressure between a liquid and the surroundings, Δp, is expressed as:

$$\Delta p = \frac{2\gamma_{lv}}{R} = \frac{2\gamma_{lv}Cos\theta}{r_k} \tag{2.4}$$

The sign and effect of Δp depends on the contact angle. For $\theta < 90°$, Δp is positive and drives the liquid into the capillary. For $\theta > 90°$, Δp is negative and represents the minimum pressure required to force the liquid into the capillary. This effect is of particular interest in the production of ceramic-metal composites. The pressure required to infiltrate a non-wetting metal into a porous ceramic can be calculated. In wetting systems the metal should spontaneously infiltrate the porous ceramic without any required external pressure.

Wetting of liquid metals on oxide ceramics

In most cases, liquid metals do not wet oxide ceramic surfaces [40]. This is thought to be due to differences in bonding type across the interface, from ionocovalent bonding in the ceramic to unsaturated bonding in the metal. There are two types of metal-oxide ceramic interactions: reactive and nonreactive. Examples of elements forming a reactive system with alumina include Ni, Si, Fe and Al [41]. Nonreactive elements include Pb, Sb, Sn, In, Ga, Ag, Au and Cu. If the metal reacts with alumina to form a metal oxide then it is reactive, else nonreactive [38]. Wetting of a pure metal on an oxide ceramic is in general enhanced by alloying with a metal with a high affinity for oxygen, e.g. Ti, or with oxygen via metal oxide or oxide atmosphere.

Wetting of copper on alumina

Copper is non-wetting on alumina. Reported values of the contact angle of copper on alumina vary between 124° [42] and 170° [41]. The pressure required to infiltrate pure copper into an alumina preform is approximately 10 to 15 MPa [33,43]. This causes the production of alumina-copper composites to be rather time-intensive and thereby expensive. By increasing the wettability of this system, it may be possible to achieve pressureless infiltration, thereby simplifying production and increasing the financial viability of the composite material [44]. Two popular methods for improving the wettability of copper on oxygen are outlined in the following paragraphs.

i) Oxygen: A copper-oxygen alloy is formed by either mixing CuO into the copper or using an oxygen-containing gas atmosphere. Varying the oxygen partial pressure between 10^{-15} and 10^{-6} leads only to a decrease in the contact angle to around 110 °. At oxygen partial pressures from 10^{-6} to 10^{-3} there is a marked decrease in contact angle to approximately 70°. Meier [45] explored the effect alloying copper with oxygen. Up to 2.5 wt.% oxygen, the contact angle decreased to 25 %. In the miscibility gap from 2.5 to 7.5 wt.% the wetting angle remained approximately constant, with a further decrease to 12 ±4° up to 11 wt.% oxygen. At the CuO-alumina interface, the formation of Cu_2O or $CuAlO_2$ has been observed [46]. The work of adhesion was found to increase with increasing weight percent oxygen [45]. A thin (1-4 μm), discontinuous layer of $CuAlO_2$ has been measured to increase the

interface strength [46], whereas a thicker (10-100 μm) layer causes a decrease in interface strength [47] due to the crack growing along the brittle $CuAlO_2$ layer.

ii) Titanium: The wettability of copper on alumina can be enhanced by alloying with titanium, which is a typical reactive wetting system [48]. Kritsalis [49] observed that the contact angle decreased to 26° as the amount of Ti was increased up to 10 mol%. Above this amount there was little change. The Cu-Ti alloy reduces the alumina surface to form a wettable reaction product TiO. Unlike the CuO-alumina system, it takes many hours for the equilibrium contact angle to be achieved since the reaction is controlled by segregation of Ti to the interface [40] and diffusion [36]. Although the equilibrium contact angle is low, spontaneuos infiltration of Cu-Ti into porous alumina has not been observed [37]. No data was found on the interface strength of Cu-Ti on alumina.

2.2.4. Residual stress, cavitation and microcracking

Regardless of how a ceramic-metal composite is produced, it is conducted at high temperatures. The metal and ceramic components generally have differing coefficients of thermal expansion, α, with $\alpha_{metal} > \alpha_{ceramic}$. When the composite is cooled to room temperature, this mismatch in α causes hydrostatic tensile stresses to form in the metal and compressive stresses to form in the ceramic [50]. This is known as residual stress. Due to its hydrostatic nature, the tensile stress in the metal component can reach levels up to 20 times the yield stress without necessarily yielding [51]. The magnitude of the residual stresses can be measured via neutron diffraction [52–54]. There is a large scatter in the residual stresses of the metal phase due to microstructural parameters: the most narrow and sharpest areas have the highest stresses which can only be relieved by plastic flow [23].

Skirl [55] explored the effect of metal content and metal ligament diameter on the measured residual stresses in the metal and ceramic phases via neutron diffraction. When the metal content was decreased, the average compressive stress in the alumina decreased and the average tensile stress in the aluminium increased. However, if the microstresses within the aluminium were taken as stress variations, it was found that the maximum value of stress was the same for all metal contents. Assuming pure elastic strain, the residual stress for a particular metal content should be independent of the metal ligament diameter. However,

Skirl found the residual stress to increase significantly with decreasing metal ligament diameter, which indicates plastic strain within the metal phase. The flow stress and thus the maximum stress achievable is increased by the increased mechanical constraint of smaller metal ligaments, which hinders yielding. For a particular ligament diameter, the maximum stress is independent of metal content. This supports that idea that the yield stress depends on the amount of constraint.

The residual stress can only be relieved by plastic flow. In composites with a strong interface, like alumina-aluminium, cavitation, that is, the formation of pores within the metal, may occur. In composites with a weak interface, like alumina-copper, the metal may delaminate from the ceramic to form microcracks [34,51]. In TEM investigations of alumina-aluminium and alumina-copper, Prielipp et al. [34] found no microcracking at the phase boundaries of alumina-aluminium, microcracking at 50 % of interfaces for a coarser structured alumina-copper (partially sintered alumina with a grain size of 4 μm) and no microcracking in a finer structured alumina-copper (partially sintered alumina with a grain size of 1.2 μm). This observation is contrary to the observation that residual stress increases with decreasing ligament diameter, since a higher amount of residual stress would be expected to lead to a higher amount of microcracking in a composite with a weak interface. In alumina-Ni_3Al microcracking was observed in up to 50% of the interfaces, concluded to be due to the weak interface [56]. Residual stress and microcracking can have a significant effect on the elastic modulus, fracture behaviour [33, 34] and the thermal expansion behaviour [23, 54, 56,57] of a composite.

2.3. Properties of ceramic-metal composites

2.3.1. Young's modulus

The Young's modulus, *E*, of metal-ceramic composites generally lies between that of the two components. Many models have been developed to describe the variation in *E* as a function of composition, depending on the composite structure, the range of composition, the ratio of the elastic moduli and the interface strength between the two components. Here, a brief description of two models is given. More exhaustive reviews include [58–60].

Rule of Mixtures (RoM): The rule of mixtures has upper and lower bounds for predicting the elastic properties of composite materials. The upper boundary, developed by Voigt [61],

assumes constant strain across the composite. For example, in a lamellar structure, this would represent the loading of the composite parallel to the boundaries between layers with the same strain in each layer. The lower boundary, developed by Reuss [62], assumes constant stress throughout the composite. In a lamellar structure, the load is applied perpendicular to the boundary between layers, with the same stress in each layer. The equations for the Voigt (U) and Reuss (L) boundaries of E are:

$$E_U = f_1E_1 + f_2E_2 \tag{2.5}$$

$$E_L = \frac{E_1E_2}{f_1E_2 + f_2E_1} \tag{2.6}$$

With f_1 and f_2 representing the volume fraction of phases 1 and 2, respectively.

These bounds represent the widest possible variation elastic modulus according to the principles of minimum potential and complementary energy. Neither of these bounds alone predict actual values for the elastic modulus, nor does this model take into account the structure of the composite.

2.3.2. Fracture toughness

Fundamentals of fracture mechanics

The following section provides a brief overview of the fracture mechanics concepts relevant to crack propagation in interpenetrating network composites. A more comprehensive explanation of mechanics theory can be found in references [60,65–67].

There are three types of loading that can be applied to a crack within a material. Mode I is tensile stress applied perpendicular to the crack plane. Mode II is shear stress applied in the direction of crack growth. Mode III is torsion stress applied parallel to the crack front. In the following, only mode I will be considered, as this is what leads to failure in most brittle materials [65].

For mode I loading in the plane of a long through crack (θ = 0) in an infinite plate, the following expression for the applied stress intensity factor, K_{IA}, in terms of crack length, c, and applied stress, σ, has been derived [65]:

$$K_{IA} = Y(c)\,\sigma\sqrt{c} \tag{2.7}$$

where $Y(c)$ is a crack length dependent shape factor describing the geometry of the crack and the mode of load applied. The shape factors for numerous experimental configurations has been analytically derived and can be found in a number of publications [60,65,68].

Early considerations of fracture mechanics were only applicable to materials displaying linear elastic behavior where Hooke's law, $E = \frac{\sigma}{\varepsilon}$, is obeyed (Linear Elastic Fracture Mechanics, or LEFM). Most materials exhibit some degree of plasticity near the crack tip, known as the plastic zone. If the plastic zone is much smaller than the thickness of the sample, the linear elastic fracture mechanics approach is still valid. For large amounts of plasticity, LEFM is inadequate and another model accounting for plasticity must be used. Crack growth occurs when the applied stress intensity factor, K_{IA}, has reached a critical value K_{I0}. This describes the stress intensity factor required to initiate crack growth in the absence any toughening mechanisms at the crack tip, that is, the crack tip toughness.

Crack initiation and growth can also be considered in terms of the energy release rate,

G. A crack can only form and grow if this causes the total energy of the system to stay constant or decrease, that is, that the energy available for crack growth is larger than the energy required to create two new surfaces [69,70]. The resistance to crack growth, R_o, is defined as work required to create two new surfaces $R_o = 2w_f$. Crack growth proceeds when G has reached a critical value:

$$G = R_o = 2w_f \tag{2.8}$$

This is analogous to K_{IO}, the crack tip toughness, described above. Equation 2.9 gives the relationship between G (or R) and K for linear elastic behaviour:

$$G = \frac{K^2}{E'} \tag{2.9}$$

Where $E' = E$ for plane stress and $E' = E/(1-\nu^2)$ for plane strain.

R-curve behavior

Materials in which two smooth surfaces are formed upon crack propagation have a constant crack resistance, that is, $R = R_o$, $K_R = K_{I0}$ (provided there is no process zone ahead of the crack tip such as phase transformation or ferroelasticity). If there are toughening mechanisms present during crack propagation, such as crack branching or bridging, the crack resistance increases with increase in crack length (Δc) according the following equations:

$$K_R(\Delta c) = K_{I0} + K_\mu(\Delta c)$$

$$or \qquad (2.10)$$

$$R(\Delta c) = R_o + R_\mu(\Delta c)$$

where $K_\mu(\Delta c)$ and $R_\mu(\Delta c)$ represent the crack length dependent contribution of the microstructure to crack resistance, also known as the microstructural shielding term.
This part contains all the crack closing stresses from the crack tip until the last intact crack bridge. K_μ and R_μ are related by the following equation [71]:

$$R_\mu = \frac{K_\mu^2 + 2K_{10}K_\mu}{E'} \qquad (2.11)$$

The energy approach allows, within limits, the elastic-plastic behaviour of crack bridging elements to be determined. The dispersed bridging energy of a crack bridging element, $R_{\mu i}$, can be calculated from the integral of the crack closing stresses, $p_i(u)$, from the crack tip to the crack opening, $u*$, at which a bridging element has failed:

$$R_{\mu i}(c) = f\int_0^{u*} pi\,[u(c)])du \qquad (2.12)$$

Where f = the area fraction of the crack bridging elements

The resistance curve or R-curve is a graphical representation of K_R or R as a function of Δc. Whether a crack grows in a stable or instable manner depends on how G and R, or K_A and K_R vary with crack length:

$$\text{stable crack growth: } \frac{dG}{dc} < \frac{dR}{dc} \text{ or } \frac{dK_A}{dc} < \frac{dK_R}{dc}$$

$$\text{instable crack growth: } \frac{dG}{dc} > \frac{dR}{dc} \text{ or } \frac{dK_A}{dc} > \frac{dK_R}{dc}$$

Stable crack growth requires increasing load to maintain crack growth, whereas instable crack growth leads to spontaneous fracture. The transition is at the point where the *G*-curve is tangent to the R-curve or the K_A curve is tangent to the K_R curve. At this point, K_A has reached a critical value of stress intensity, K_{IC}, called the fracture toughness. G_{IC} is analogous. K_R can be determined experimentally, as long as the Young's modulus of the material is known. This is advantageous when the shape factor of the given material and loading conditions cannot be determined analytically.

Determination of crack tip toughness and the microstructural shielding term

The crack tip toughness of a material is an important parameter representing the stress intensity factor when crack growth begins. In practice it is difficult to measure directly, since crack extension measurements are usually measured starting from a notch or a sharp crack that has be cut to make it a short crack (to remove the bridged zone). This method was developed by Steinbrech and Knehans [72] in order to measure the R-curve behaviour of alumina as a function of grain size. However, in this method it is essential to have a continuous crack front. This necessitates a minimum crack length of 100 to 200 μm, where it is not possible to ignore the effects of a crack bridging region.

Fett et al. [73] developed a method to determine K_{IO} using a strain gauge to detect the first deviation from linearity in the load-displacement measurement of a V-notched beam under four-point loading. K_{IO} can also be determined by measuring the profile of a crack under load, also called **c**rack **o**pening **d**isplacement or COD. The width of the crack is measured from the tip of the crack, through the bridged region to well within the unbridged region of the crack. Ideally this would be measured at the critical load. However, since this would lead to crack extension, the crack profile is measured at one or more loads below the critical load and extrapolated to the critical load. Using the Irwin equation [74], K_{IO} can be calculated by fitting an appropriate function to the first 50 to 100 μm of the crack profile (equation 2.13):

$$u(x) = \frac{K_{IO}}{E'} \sqrt{\frac{8x}{\pi}} \tag{2.13}$$

Results obtained with the COD method have shown that the strain gauge technique overestimates K_{IO} [75]. Kounga et al. [76] developed a more rigorous mathematical approach based on the Irwin equation. It takes the whole of the measured COD into account when calculating K_{IO}. However, since this yielded similar results to the Irwin approach, the simpler Irwin approach is used in this work. Different methods used to measure the crack profile include optical interference [77], SEM [78], Raman microscopy [79] and atomic force microscopy [80]. Once K_{IO} has been determined, $K_{\mu}(\Delta c)$ can thus be determined according to equation 2.11.

2.4. Toughening mechanisms

There are two broad categories of toughening mechanisms: process zone mechanisms and crack bridging mechanisms. In some ceramic materials and CMCs the high stress at the crack tip triggers particular processes in a finite area around the crack tip. This is known as a process zone. Some examples are localised microcrack formation (which in contrast to thermally induced microcracks do not weaken the material), phase transformation or ferroelastic domain switching. As the crack grows into the process zone, this zone applies closure stresses to the crack wake such that a higher load is required for further crack propagation. Since this category is not relevant to alumina-copper composites, this will not be dealt with further. Of particular relevance are crack bridging mechanisms. These have been discussed in detail by Rödel [71]. The four major categories are: i) elastic or intact bridges, ii) plastic or friction bridges, iii) elastic-plastic or mechanically interlocking bridges and iv) ductile bridges. These categories are illustrated in figure 2.5.

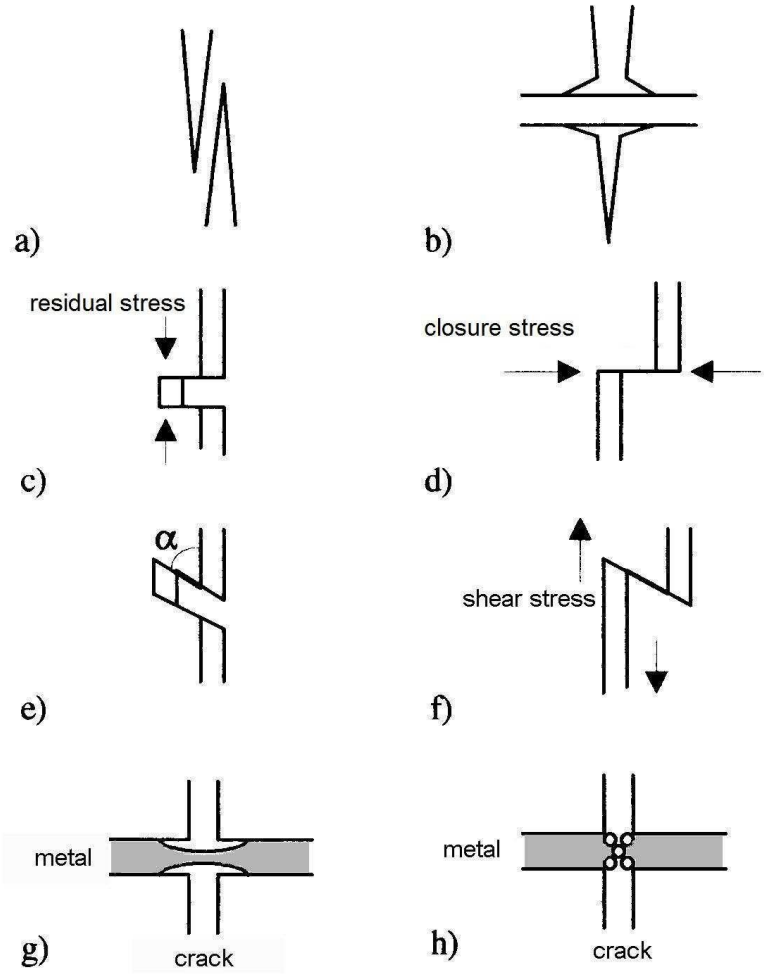

Figure 2.5: Schematic representation of possible bridging mechanisms: a) and b) intact (elastic) bridges with a) constant delamination length and b) increasing delamination length; c), d) friction (plastic) bridges of different geometries; e) and f) different forms of mechanical interlocking; ductile bridges with failure due to g) necking or h) cavity formation [71].

In interpenetrating metal-ceramic composites, the dominant toughening mechanism is due to ductile bridging. Many aspects of the metallic bridges can affect the toughening behaviour:

1. the morphology including metal ligament diameter, ligament orientation and metal content
2. the properties of the metal like yield strength, Young's modulus and ductility
3. the interaction between the metal and ceramic phases including interface strength and difference in thermal expansion coefficients

By tailoring the microstructure of the metallic network via the porous ceramic preform it is possible to influence the $p(u)$ function and thus the mechanical properties of the composite. The influence of the metal ligament diameter on the $p(u)$ function and the R-curve is shown in figure 2.6. During crack propagation finer metal ligaments lead to a steeper $p(u)$ curve with a smaller critical crack opening at which the ligament fails. The area under the curve is proportional to the energy absorbed by the bridging elements. Finer ligaments can only accommodate limited dislocation motion (plastic deformation) and thus only dissipate a limited amount of energy. In coarser metal ligaments more dislocation motion is possible, thus the plastic deformation and dissipated energy is larger. This leads to smaller crack closure stresses for a given crack opening and an increase in the critical crack opening. The initial slope of the $p(u)$ curve is reduced, while the peak value remains constant and is shifted to a higher u. Similarly, the slope of the R-curve is also lower. The plateau value of crack resistance is higher since the coarse ligaments are able to accommodate more strain. The fracture toughness is higher due to the higher plateau but the fracture strength lower due to the lower slope of the R-curve.

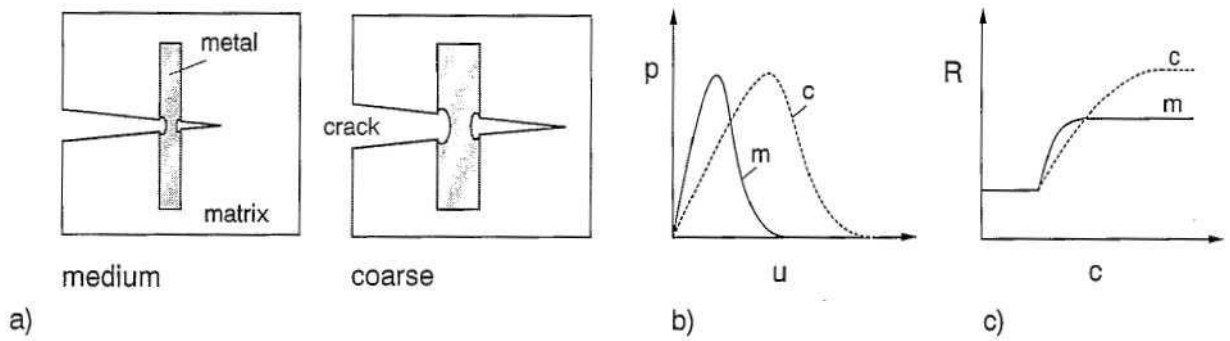

Figure 2.6: Schematic diagram describing b) p(u) functions and c) R-curves for metal reinforced ceramics with varying metal ligament diameter a), based on the assumption of scale independent metal deformation [34].

The effect of metal content on the R-curve is shown in figure 2.7. With increasing metal content both the slope and the peak of the R-curve are higher. For a constant metal ligament diameter, with increasing metal volume fraction, the ligaments must be closer together, resulting in a steeper slope. A higher metal content means that more energy is absorbed by plastic deformation, hence the higher plateau. Thus with increasing metal content, both the fracture toughness and fracture strength increase.

Not just the morphology of the composite effects the $p(u)$ curves; the properties of the metal phase also play a role. The yield strength, Young's modulus and ductility of the metal phase also have an effect on the $p(u)$ function. A higher yield strength enables each ligament to withstand a higher stress before failing, thus increasing the peak value. A higher Young's modulus would increase the initial slope of the $p(u)$ curve, analogous to a stress-strain curve. An increased ductility would enable each ligament to plastically deform further and absorb more energy before failing, thus shifting the peak of the $p(u)$ curve to higher u values.

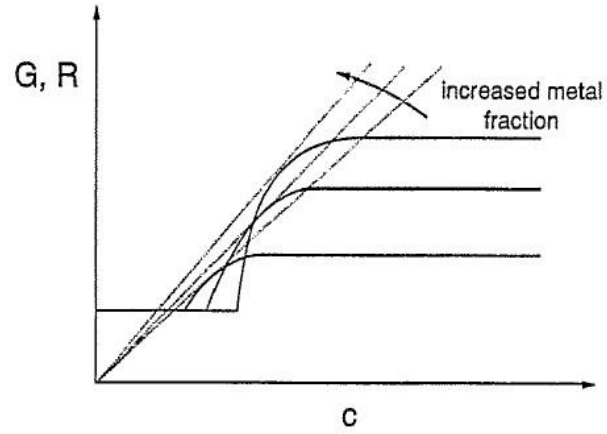

Figure 2.7: Schematic diagram describing the effect of metal fraction on the R-Curve [34].

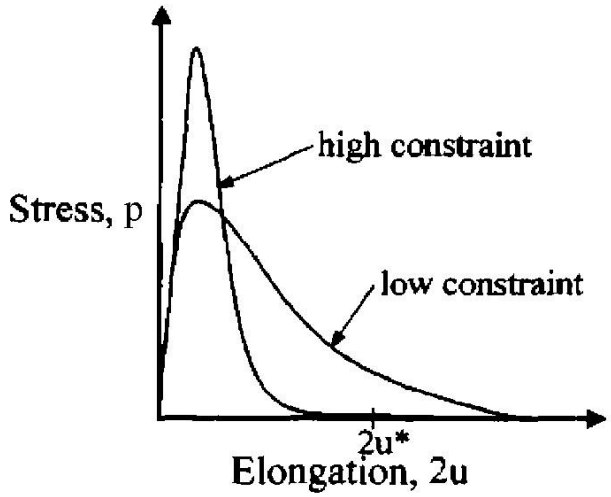

Figure 2.8: Schematic diagram describing the variation in the p(u) function with varying constraint of the metallic phase [81].

The interaction between the metal and ceramic phases also influences the $p(u)$ curve. A high interface strength means that the metal ligaments are highly constrained and vice versa. The effect of mechanical constraint is shown in figure 2.8. A low interface strength between the two phases causes delamination between the metal ligament and the ceramic during crack propagation. The length of the ligament able to plastically deform is longer, meaning more

energy can be dissipated leading to a higher toughness value. The higher the difference in thermal expansion coefficient between the metal and ceramic phase, and the higher the processing temperature, the more thermal residual stress is present within the composite. This is before any external load is applied. The compressive stress present in the ceramic phase is advantageous, since more opening stress can be applied before the compressive stress is reversed and the tensile stress for crack growth is reached. The tensile stress present in the metallic phase would allow for less elastic deformation before the yield stress is achieved and plastic flow occurs.

2.5. Thermal expansion and conductivity

Thermal strain

In homogeneous materials, the strain-temperature curves generally follow the same path for heating and cooling. In metal-ceramic composites the thermal expansion behaviour is more complicated. Skirl et al [23] found the strain curves of interpenetrating alumina-aluminium composites to be hysteretic, with the strain curve higher upon heating and lower upon cooling. The total strain increased linearly with metal content, but the amount of hysteresis was unaffected. The hysteresis was proposed to be due to one or more of the following reasons: i) flow of metal into residual porosity, ii) microcavitation in the metal phase formed during cooling after production, or iii) intrusion/extrusion of metal ligaments at the surface of the sample ($\approx 6.5\ \mu$m). Hoffman et al [57] explained the results from Skirl et al using two different models. The first approach was a macroscopic consideration of the total composite strain based on the variation of stress in the metal phase during thermal cycling. The second approach was a micromechanical consideration of time-dependent effects in the metal phase, such as creep. Figure 2.9 a) is a representation of the effect of stress and plastic flow in aluminium upon macroscopic thermal expansion. This describes the typical hysteretic strain curve of the alumina-aluminium composites. Figure 2.9 b) schematically shows the variation of stress in aluminium as a function of temperature. The different regions in the curve are explained in detail in [57] so only a brief description of regions 1 to 5 will be given here.

Curve 1: Starting at T_{visc}, upon cooling the metal shrinks elastically and tensile stress builds up.

Curve 2: There is a decrease in the slope of the curve when the tensile yield stress of the metal is reached with further strain requiring plastic deformation. The stress in the metal remains constant. Here cavitation or delamination may occur.

Curve 3: Upon reheating the metal expands elastically and is parallel to curve 1. The tensile stress in the metal is reduced to zero and compressive stress builds.

Curve 4: When the compressive yield stress of the metal is reached the slope of the curve decreases and the stress in the metal remains constant. The balance between thermal strain and gradual reduction of plastic strain leads to the slope of the curve (CTE) being less than that of pure alumina.

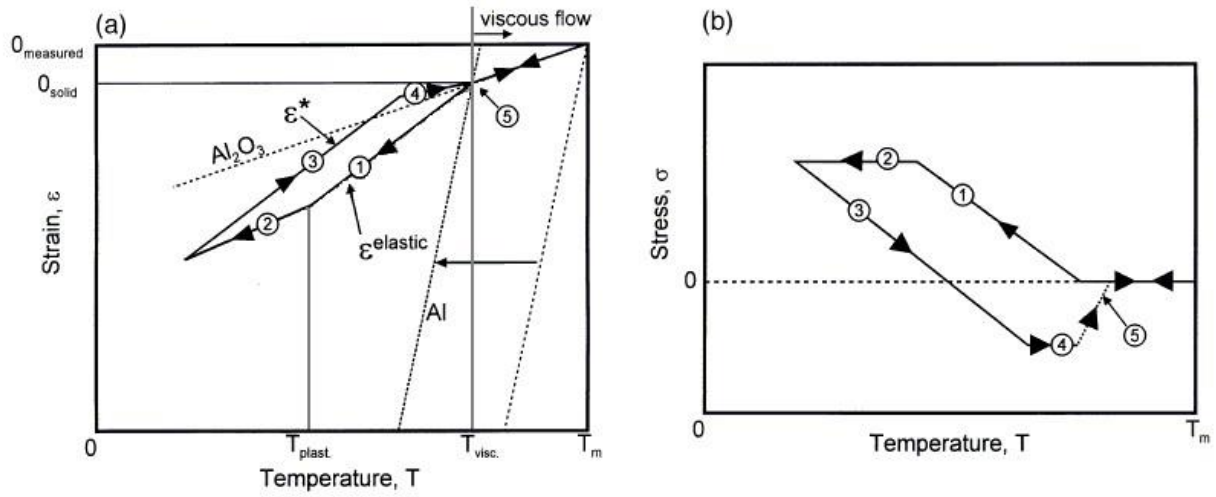

Figure 2.9: (a) Schematic representation of the effect of plastic flow in the aluminium upon macroscopic strain ǫ∗ and the application of approach 1 to calculate (b) stress in the metal phase as a function of temperature [57].

Curve 5: T_{visc} has been reached as the metal flows viscously, leading to a relaxation of stress to zero. The slope of the composite strain curve approaches that of pure alumina.

The second model considered the effects of different creep mechanisms at different temperatures, but was acknowledged to be inappropriate in the case of extensive cavitation or microcracking, as might be expected in alumina-copper. It was concluded that the plastic

deformation of the metal was largely due to diffusion based processes at high temperatures and a limited amount of cavitation yielding close to room temperature.

Alumina-aluminium has a strong interface whereas alumina-copper does not. Since no publication on the thermal strain behaviour of alumina-copper were found, the thermal strain behaviour of another system with a weak interface, alumina-Ni_3Al, is briefly described here. Skirl et al. [56] found there to be no hysteresis in strain curve up to 900 °C. Between 900 and 1000 °C there was a small hysteresis. It was presumed that there was only elastic deformation of Ni_3Al below 900 °C and that the weak interface prevented a stress build up. For the same reason it was assumed there was only a minimal amount of residual stress present after production, although this was not measured. The total strain increased with increasing Ni_3Al content, but the amount of hysteresis was not significantly affected.

Coefficient of thermal expansion (CTE or α)

CTE is calculated either as an average value across a particular temperature range, ($\Delta\varepsilon/\Delta T$), or as an instantaneous value, ($d\varepsilon/dT$), and is often plotted against temperature. There are a number of different models to predict the variation in CTE with composition in two component composites. The simplest is the Wiener model [82,83], analogous to the rule of mixtures (RoM), but derived for thermal and electrical properties. In equation 2.5, E is simply replaced with α. This assumes that both phases are able to slide freely and do not exert a force upon each other. There are two different models to predict the CTE of composites with a strong interface, where both phases deform elastically; the Kerner and Turner models.

i) The Kerner model [84]: considers a spherical particle of one phase enclosed by a matrix (perfectly bonded), as in an MMC or a CMC. By using an averaging procedure due to Bruggeman [85], and analysing the effect of a uniform hydrostatic compression and of a uniform tension on an average grain, an equation for the bulk modulus was found. The composite CTE was found from an analysis of the dilatation and bulk stress when the composite as a whole is subjected to some small temperature change:

$$\alpha = f_1\alpha_1 + f_2\alpha_2 + \left[\frac{4G_2}{K_C}\right]\left[\frac{(K_C - K_1)(\alpha_2 - \alpha_1)f_1}{4G_2 + 3K_1}\right] \qquad (2.14)$$

Where subscript 1 and 2 represent the outer phase and inner phase, respectively, K is the bulk compression modulus, G is the shear modulus and K_c is the bulk compression modulus of the composite.

The Turner model [86]: a purely hydrostatic stress is applied and it is assumed that there is a homogeneous strain across the composite. No shape factor is taken into account. This was one of the first models for composite CTE that took the elastic constants of the constituent phases into account. This model would be expected to be more suitable for interpenetrating composites [23, 87], since the interpenetrating structure would cause constraint of each phase such that the strain should be homogeneous throughout the sample, which is not the case with MMCs or CMCs (Kerner model). The equation for the composite CTE is:

$$\alpha = \frac{f_1 K_1 \alpha_1 + f_2 K_2 \alpha_2}{f_1 K_1 + f_2 K_2} \tag{2.15}$$

Hsieh et al. [88] measured the thermal expansion behaviour of alumina-Ni_3Al composites from 0 to 100 % alumina and found the Kerner and Turner models the only bounds to be able to encompass all experimental data.

Thermal conductivity

The most important mechanism of heat transfer in solid materials is conduction. The ability of a material to transport heat is described by λ, the thermal conductivity (unit W/mK). This describes the heat flow, dQ/dT, through the cross section of a material with an area, A, that is under a temperature gradient of dT/dx. The relationship is analogue to the equation for diffusion:

$$\frac{dQ}{dt} = \lambda A \frac{dT}{dx} \tag{2.16}$$

Thermal conductivity can be measured using either steady-state methods or transient methods.

i) Steady-state: In steady state methods, the temperature difference across a sample is constant. For example, if a temperature difference, ΔT, across a sample of length, L, and

cross section, *A*, is applied using electrical power ($P = V^2/R$) with a known voltage, *V*, and resistance, *R*, in ohms, to supply the heat flow $dQ/dt = P$, equation 2.16 can be rearranged to calculate the thermal conductivity:

$$\lambda = \frac{V^2 L}{RA\Delta T} \quad (2.17)$$

This method is mathematically simple, however, requires a constant temperature difference across the sample to have been achieved. This can be time consuming.

ii) Transient: In transient methods, the change of temperature over time is measured. The differential equation for heat transport is analogue to Fick's second law of diffusion:

$$\frac{dT}{dt} = a\frac{\partial^2 T}{\partial x^2} \quad (2.18)$$

where *a* is the thermal diffusivity of the material. To determine thermal conductivity, the following relationship is used:

$$\lambda = a\rho C_p \quad (2.19)$$

where C_p is the heat capacity and ρ the density of the material. One such method is the 'Laser-flash' method [89]. A thin disk-shaped sample is heated on one side with a short laser pulse and the change in temperature on the other side is detected with an infrared detector. This method is much faster than any steady-state method, however, mathematically more complicated.

The thermal conductivity of a material is strongly influenced by its microstructure. Any defects, pores or microcracks can significantly decrease the conductivity. If the material is anisotropic, the conductivity will also be anisotropic. In composites, the thermal conductivity will be between that of the phases composing it. The interface between phases also effects the conductivity. The interface itself is a barrier to heat flow. Any delaminated areas on the interface cause a significant decrease in conductivity, since the thermal conductivity of air is much lower than that of typical solids.

The variation of thermal conductivity with composition in a two phase composites can be described by a number of models. As in CTE, the Wiener model [82,83], analogous to the rule of mixtures (RoM), can be used. In equations 2.5 and 2.6, E is simply replaced with λ.

The Hashin-Strikman bounds: Using similar principles to the derivation of the bounds for elastic properties (section 2.2.1), Hashin and Strikman [90] also developed bounds for thermal and electrical properties that can be applied to thermal conductivity. The equations for the upper (U) and lower (L) bounds are:

$$\lambda_{HS-U} = \lambda_2 + \frac{f_1}{\frac{1}{\lambda_1 - \lambda_2} + \frac{f_2}{3\lambda_2}} \tag{2.20}$$

$$\lambda_{HS-L} = \lambda_1 + \frac{f_2}{\frac{1}{\lambda_2 - \lambda_1} + \frac{f_2}{3\lambda_1}} \tag{2.21}$$

where the subscript 1 and 2 represents the phases with the lower and higher thermal conductivity, respectively.

The Lichtenecker average

Lichtenecker [91] was the first to consider an interpenetrating composite geometry in the modelling of electrical and thermal properties of composites. It is based on a unit cell of a cube with one phase located at the edges of the cube, the other phase within the cube. An elegant averaging formula was derived based on slicing the microstructure into many thin slices and considering either infinite conductivity surface between two slices, or infinite resistance. These two conditions ultimately lead to a combination of mixing rules, like RoM. The general equation is:

$$K_C = K_1^{f1} + K_2^{f2} \tag{2.22}$$

where K stands for any material constant, subscript C for composite, subscripts 1 and 2 for the two components and f the volume fraction of the respective component. This formula is basically a generalized geometric mean. It has been shown to match many experimental results dielectric constants, the light refraction indices, thermal conductivities and electric resistivities [92].

2.6. Fracture toughness

The common interpretation of the plane-strain fracture toughness K_{IC}, defined by ASTM E 399, is a specimen size insensitive lower bound fracture toughness corresponding to plane-strain stress state. The interpretation is due to the original work by George Irwin where he postulated the expected effect of specimen thickness on fracture toughness. George Irwin based his conclusions on maximum load toughness behavior of center cracked tension specimens of two aluminum alloys, combined with the specimens macroscopic fracture surface appearance [93]. The choice of method for determining the fracture toughness depends on the availability of time, resources and level of precision required for the application. In practice, measurements of KIC require certain microstructural conditions on the material to allow propagation of cracks through it in a consistent manner. The strength of materials is governed by the known theory of Griffith, [94] which relates the strength (S) with the size of the defect or crack (c) by: $S = YK_{IC}/c^{1/2}$. One particularly attractive procedure due to its simplicity for routine evaluations of engineering materials is the indentation fracture (IF) method. Although the IF method can only measure approaches of the values of K_{IC}, is a convenient technique for evaluation of many brittle engineering materials. This technique is based on normalized standards hardness tests. [95, 96]

2.7. Alumina-metal composites

Dominique Osso et.al, [97] reported that the synthesis of powder $A1_2O_3$-metal composites can be performed by room temperature ball-milling of mixtures of metal-oxides and aluminum. Such composites may also be prepared by direct grinding of a mixture of $A1_2O_3$ and of a metal or an alloy to improve the mechanical properties.

2.7.1. **Alumina-titanium composite**

Sergio J. Esparza-Vázquez et.al, [98] on their study on Strengthening of Alumina-Based Ceramics with Titanium Nanoparticles, reinforce titanium particle on alumina to increase its fracture toughness. Alumina is a very useful ceramic because of its wide variety of applications [99]. Its use is mainly due to its high hardness and compression strength as well as high electrical and thermal insulation properties. Furthermore, its uses range from the manufacture of cutting tools and medical implants to the manufacture of insulating materials both electrical and thermal. However, due to their low resistance to fracture, which is a common feature of all ceramic materials, their utility has not been expanded [100]. In order to reduce the brittleness of alumina, other studies have prepared different matrices of alumina ceramics strengthened with metallic particles, and demonstrated that the size and

uniform distribution of the particles in the ceramic matrix contributed to obtain composites with good mechanical properties, and especially increased fracture toughness [101]. One of the main problems of the previously mentioned systems is that sophisticated processing techniques are employed for the production of composites, which involves expensive and often few productive processes. Enrique Rocha-Rangel et.al, [102] showed that Strengthened Al_2O_3-based composites can effectively be reinforced by inducing fi ne dispersions of TiC/Ti, throughout a combination of experimental techniques, such as; mechanical milling, pressureless sintering PLS (Aratmosphere) and cementation process (vacuum). The later provided that Al_2O_3, Ti and activated carbon fine precursor powders are bring together as to react upon sintering forming a functionally graded- cemented layer. This *in-situ* synthesis method produces composites that are greatly sinterable and do exhibit enhanced toughness, as compared to monolithic-Al_2O_3 ceramics. This toughening improvement technique offers the possibility of a low synthesis cost, turning into an attractive synthesis route for scaling the process up to a pilot plant-level. N. Travitzky et.al, [103] reported Crack deflection by alumina grains and crack bridging by the more ductile intermetallic may control the fracture toughness of these composites. Dense alumina–TiAl–Ti_3Al composites were fabricated by thermal explosion (SHS) of TiO_2–Al powder blend performed in a rigid die under a low applied pressure.

2.7.2. **Alumina-copper composite**

E. Rocha-Rangel and J. G. Miranda-Hernández [104] studied the fracture toughness of Alumina-Copper Composites through an intense mixing process of Al_2O_3 powder with different copper contents. It becomes significant that, the copper metallic phase is more noticeable, found forming elongated thin shapes in the grain surroundings in the alumina matrix that are shaping partially the metallic net as a result of the copper increase in the composition, which is taking up some of the porosity spaces in the porosity, thus diminishing it. Their study shows that, in Al_2O_3-10% Cu composite, the metallic network is still partial and isolated, although is more visible due to the greater metal content in the composition. Another appreciably observation is the growth of both grains and pores size, and in Al_2O_3-20% Cu composite the grain in the microstructure is now bigger, the pores are larger but their number has diminished.

The liquid helps to obtain dense composites because it goes into the material's bulk filling the sites previously occupied by pores, thus forming an interpenetrating network with the

ceramic matrix. At this respect, it is important to mention than several authors [105, 106] have documented good wetting of Al_2O_3 ceramic by liquid copper.

2.7.3. **Alumina-graphene composite**

High-frequency induction heat sintering (HFIHS) technology was employed for fabrication of highly dense (>99.5%) graphene-reinforced alumina nanocomposites. The mixed powders were consolidated at temperatures up to 1500 °C with 0.25 to 3.0 wt.% exfoliated graphene n''anosheets (GNS). Compared with monolithic alumina, there was grain size refinement by 46%with an associated increase in the fracture toughness (by 72%) and hardness values (7%). Electron microscopy revealed that exfoliated GNS retained their inherent planar structure against any possible chemical and/or thermal adverse effect caused by rapid sintering. The intrinsic 2- dimensional sheet morphology and flexibility of the GNS promoted formation of large Al_2O_3/GNS interfacial area, thus leading to a dominant reinforcing mechanism via grain anchoring. The presence of GNS at the grain boundary areas not only inhibited grain growth through pinning effect, it also modified friction traits at nanoscale level by inducing slip–stick phenomenon that increased the Al_2O_3/GNS interfacial strength by means of improved efficiency of graphene pull-out and crack-bridging that subsequently imparted toughness and altered the failure behavior of the composites. A possible correlation between GNS incorporation into Al_2O_3 matrix and the resulting mechanical properties is established through high-resolution TEM studies that indicated graphene/alumina interface formation without any presence of severe intermediate phases.[107]

2.7.4. **Alumina/zirconia-silver composite**

Jerome Lalande et.al, [108] reported that attrition milling of alumina and silver in acetone leads to slightly finer and more homogeneous Ag distribution in the alumina matrix than when water is used. An ultrafine alumina powder is detrimental for refining the mixture. The strength of a 10 vol.% Ag material is 590 MPa, similar to that of the corresponding ZrO_2– Al_2O_3 ceramic, and fracture toughness is higher: 5.1 MPa $m^{1/2}$ compared to 4.6 MPa $m^{1/2}$ without silver addition. It is not possible to get interconnected metal inclusions with this system because silver vaporizes during sintering. High amounts of silver degrade the mechanical resistance. However, the toughness enhancement achieved by crack bridging is still observed by incorporating 20 vol.% silver.

2.7.5. **Alumina-Aluminium composite**

K. Konopka and M. Szafran [109] studied the fabrication of Al_2O_3–Al composites by metal infiltration into porous preforms. This technique allows to obtain homogeneous distribution of metallic phase in the ceramic matrix. The pores were nearly fully infiltrated by metal. Using Ni–P coating on ceramic preforms improved wetting Al_2O_3 by Al. Ni–P were deposited in form of a thin, tight film, which encapsulated ceramic grains. The wetting behavior between aluminium and alumina with and without Ni–P coating showed interaction between Al and Al_2O_3 coated by Ni–P layer. This interaction leads to bonding in a contact area. As a consequence, during the process of infiltration the liquid Al contacts first with Ni and then migrates inside porous preform. However, the process of Al released caused by pressing is observed. This effect should be taken into consideration in designing of composites (in calculation of the amount of Al which is needed for full infiltration). During the process of infiltration, the new phases appeared. Among them, there are spinel phase and aluminides. These phases are an evidence of diffusion reaction between liquid aluminium and alumina. As a consequence, they can influence the fracture toughness of the composites. Green compaction of samples plays a fundamental role in fabrication of alumina/aluminum composites. Vibration is found an inappropriate method in this respect. It is found that density increases while porosity decreases as a result of the sintering and the oxidation reaction proceeding. No significant changes in the density and porosity are observed in the range of sintering temperatures selected. On the other hand, the expansion due to oxidation can overcome the shrinkage determined by sintering and the volume of samples increases, while the density decreases. The strength of the composites increases with temperature increase because of porosity decrease brought about by the sintering progress. [110]

CHAPTER 3 MATERIALS AND METHODS

3.1. Material selection

Alumina powders

A high purity alumina (Sigma-Aldrich, 99.5% purity, 210μm) was chosen as the main matrix material for this study. It does not need to be very fine in order to give a pore channel diameter large enough to be infiltrated with Titanium and copper.

Titanium/Copper

A high purity Titanium (Sigma-Aldrich, 98.8%, 200μm) and copper (Sigma-Aldrich, 99.8%, 200mesh, free of oxygen and phosphorous) was chosen as the metallic reinforcement of these interpenetrating ceramic-metal composites for a number of reasons. Firstly, titanium, however it has a low density, its higher strength gives a high fracture toughness to alumina. Secondly, a high thermal conductivity was one of the target properties. Copper was chosen since it gives the best of the two properties, fracture toughness and conductivity, together than any of the metals do. The high ductility of copper (60 % elongation to break at room temperature) makes it a good candidate for providing a high fracture toughness in a composite. The wettability of copper on alumina can be enhanced by alloying with titanium, which is a typical reactive wetting system (see chapter 2.2.3), so that the reinforced metallic particles can easily penetrate in to the pores of the matrix and fills out the pore inorder to reduce its volume which then results in a better density and enhanced fracture toughness.

Figure 3.1: Starting materials i.e. Ti/Cu/Al_2O_3 from left to right

3.2. Material preparation and Synthesis

Five different compositions, Al_2O_3 being the principal component, whereas the content of Ti and Cu varied according to the following contents: (0.0 wt %, 3.0 wt %) and (0.0 wt %, 1.0 wt %, 2.0 wt %, and 3.0 wt %) were first prepared by weighing the powders using a weighing balance in the desired proportion and mixed with alumina.

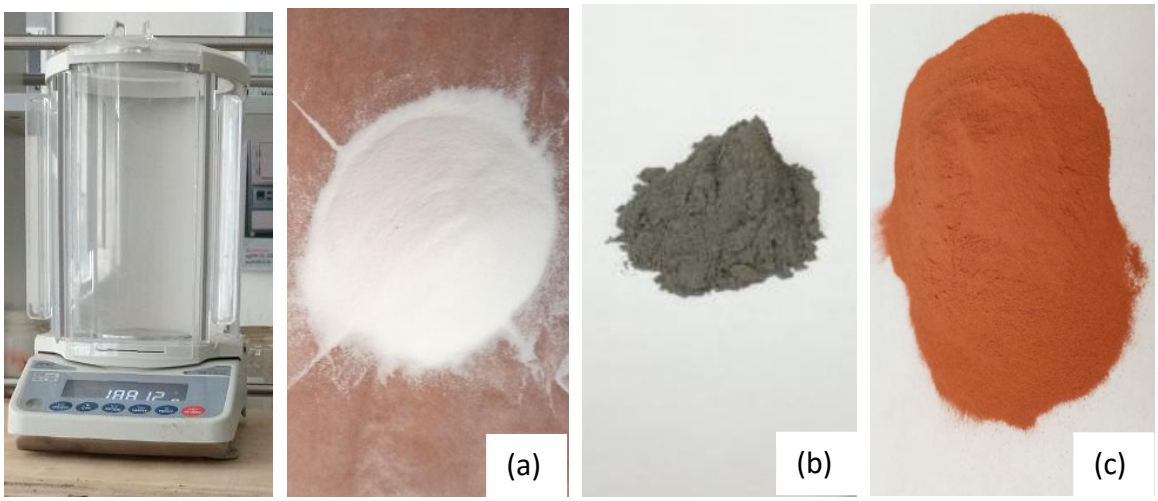

Figure 3.2: A weighing balance and powders of a) Alumina b) Titanium c) Copper

Table 3.1: The proportion of reinforced metals, Ti and Cu to that of matrix Al_2O_3

Compositional proportion	Al_2O_3 (wt %)	Ti (wt %)	Cu (wt %)
1	100.0	0.0	0.0
2	97.0	3.0	0.0
3	96.0	3.0	1.0
4	95.0	3.0	2.0
5	94.0	3.0	3.0

There were a total of 30 samples prepared for the different sintering time and sintering temperature values.

Miling

These compositions were processed by high energy milling using a planetary mill type (Planetary mono mill Pulverisette 6) with ZrO_2 grinding elements of 1 cm and 2.5 cm diameter and a cylindrical stainless steel vessel with a volume of 250 ml. The milling was carried out for 6 hours at 250 rpm in dry. The powder weight/ball weight ratio was 1:14, using the volume of 1/3 of the container.

Green body formation

Cylindrical samples of each composition with 2 cm and 0.45 cm of diameter and thickness respectively, were compacted using 65 MPa pressure, with the aid of a uniaxial press. The powders let to compact into a rigid die by applying a 65 MPa pressure in a single axial direction through a rigid piston with a 60 second holding time.

Figure 3.3: Pressed green bodies of monolithic Alumina and Alumina-Ti/Cu composites

Sintering

For a very good compaction, a reduced porosity and better densification, the green samples were sintered in an electric tube furnace at 1300˚C, 1200ºC and 1100ºC for 2 and 3 hours. In all cases, a heating rate of 10˚C/min and a volumetric flow of nitrogen gas of 15 cm^3/min in the furnace combustion chamber were employed. The sintering temperatures of composites must be lower than the melting temperature of the matrix material, in this case Al_2O_3.

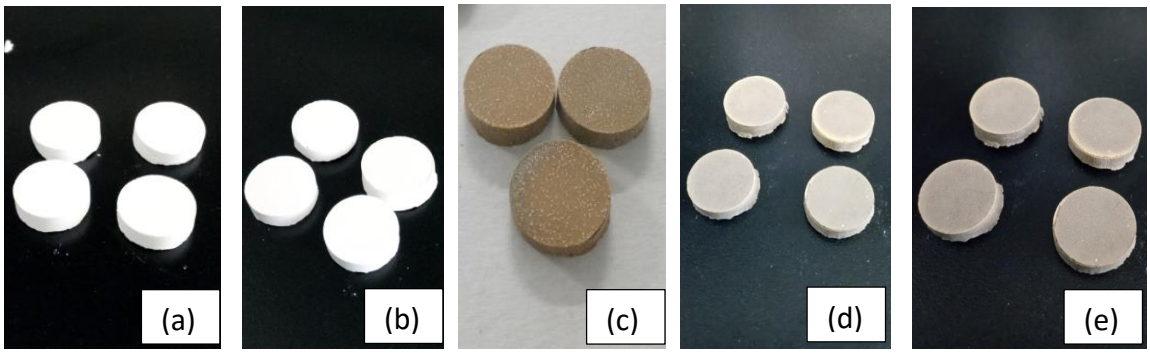

Figure 3.4: Sintered samples a) Al_2O_3, b) Al_2O_3-3%Ti, c) Al_2O_3-3%Ti-1%Cu, d) Al_2O_3-3%Ti-2%Cu e) Al_2O_3-3%Ti-3%Cu at different sintering temperature and time range.

3.3. Sample nomenclature

Based on the reinforced metals (Titanium and copper) and their volume fraction, the apparent sintering time and temperature, the following sample nomenclature will be used from this points onwards:

A1=Al_2O_3 sintered for 2 hours at 1100 ^{0}C

A11=Al_2O_3 sintered for 3 hours at 1100 ^{0}C

A2=Al_2O_3 reinforced with 3wt% Ti sintered for 2 hours at 1100 ^{0}C

A21=Al_2O_3 reinforced with 3wt% Ti sintered for 3 hours at 1100 ^{0}C

A3=Al_2O_3 reinforced with 3wt% Ti-1wt% Cu sintered for 2 hours at 1100 ^{0}C

A31=Al_2O_3 reinforced with 3wt% Ti--1wt% Cu sintered for 3 hours at 1100 ^{0}C

A4= Al_2O_3 reinforced with 3wt% Ti-2wt% Cu sintered for 2 hours at 1100 ^{0}C

A41= Al_2O_3 reinforced with 3wt% Ti-2wt% Cu sintered for 3 hours at 1100 ^{0}C

A5= Al_2O_3 reinforced with 3wt% Ti-3wt% Cu sintered for 2 hours at 1100 ^{0}C

A51= Al_2O_3 reinforced with 3wt% Ti-3wt% Cu sintered for 3 hours at 1100 ^{0}C

B1= Al_2O_3 sintered for 2 hours at 1200 ^{0}C

B11= Al_2O_3 sintered for 3 hours at 1200 ^{0}C

B2= Al_2O_3 reinforced with 3wt% Ti sintered for 2 hours at 1200 ^{0}C

B21= Al_2O_3 reinforced with 3wt% Ti sintered for 3 hours at 1200 ^{0}C

B3= Al_2O_3 reinforced with 3wt% Ti-1wt% Cu sintered for 2 hours at 1200 ^{0}C

B31= Al_2O_3 reinforced with 3wt% Ti-1wt% Cu sintered for 3 hours at 1200 ^{0}C

B4= Al_2O_3 reinforced with 3wt% Ti-2wt% Cu sintered for 2 hours at 1200 ^{0}C

B41= Al_2O_3 reinforced with 3wt% Ti-2wt% Cu sintered for 3 hours at 1200 ^{0}C

B5= Al_2O_3 reinforced with 3wt% Ti-3wt% Cu sintered for 2 hours at 1200 ^{0}C

B51= Al_2O_3 reinforced with 3wt% Ti-3wt% Cu sintered for 3 hours at 1200 ^{0}C

C1= Al_2O_3 sintered for 2 hours at 1300 ^{0}C

C11= Al_2O_3 sintered for 3 hours at 1300 ^{0}C

C2= Al_2O_3 reinforced with 3wt% Ti sintered for 2 hours at 1300 ^{0}C

C21= Al_2O_3 reinforced with 3wt% Ti sintered for 3 hours at 1300 ^{0}C

C3= Al_2O_3 reinforced with 3wt% Ti-1wt% Cu sintered for 2 hours at 1300 ^{0}C

C31= Al_2O_3 reinforced with 3wt% Ti-1wt% Cu sintered for 3 hours at 1300 ^{0}C

C4= Al_2O_3 reinforced with 3wt% Ti-2wt% Cu sintered for 2 hours at 1300 ^{0}C

C41= Al_2O_3 reinforced with 3wt% Ti-2wt% Cu sintered for 3 hours at 1300 ^{0}C

C5= Al_2O_3 reinforced with 3wt% Ti-3wt% Cu sintered for 2 hours at 1300 ^{0}C

C51= Al_2O_3 reinforced with 3wt% Ti-3wt% Cu sintered for 3 hours at 1300 ^{0}C

For example, sample C31 is alumina reinforced with 3wt% titanium and 1wt% copper, which is then sintered for 3 hours at 1300^{0}C.

3.4. Characterization

3.4.1. Microstructure and composition

The samples were examined in an optical microscopes and their images were analyzed to observe the morphology of the composites.

3.4.2. Density

The density of both the green body, the compacted preform before sintering, and the samples after sintering was estimated with Archimedes' principle which aids the determination of density by providing a convenient and accurate method for determining the volume of a solid object whatever its shape is, whether it is regular or irregular.

For all the samples prepared for this study, their weight in the air (m) is measured and then submerged in water and their weight in water (m_1) is also recorded. It is clear that it has displaced the difference between the weight in air and the weight in water ($m-m_1$) gram of water. Since water has a density of 1 gram/cm^3, this implies the volume of the object (v) would be the value of the displaced water in cm^3, so that the density of the object (ρ) is then the ratio of its mass in air to the volume of the displaced water:

$$\rho=m/v \tag{3.1}$$

3.4.3. Mechanical Properties

3.4.3.1. Young's modulus

The Young's modulus, *E*, of metal-ceramic composites generally lies between that of the two components. The value of *E* was determined as a function of the composite composition, using the equations of the Voigt (U) and Reuss (L) boundaries of *E*.

3.4.3.2. Hardness

Hardness was tested with a Vickers hardness tester (HVS-50). It was tested under a load of 10 N for 15 sec indentation holding time. This was to ensure that the indentation covered an area representative of the composite. Three indentations were made on each sample and lengths of the diagonals of each indentation (d_1 and d_2, average value d in mm) indentation used to calculate hardness, *HV* (GPa) according to equation 3.2:

$$HV=1.8544\frac{F}{1000d^2} \tag{3.2}$$

3.4.3.3. Fracture toughness

The fracture toughness of the samples was determined from the hardness value obtained from the Vickers indentation using the equation of fracture toughness evaluation from Vickers indentation by Niihara which is the most common method of finding fracture toughness from indentation.

$$K_{IC}=0.00165E^{0.4}F^{0.6}a^{-0.7}\left(\frac{c}{a}\right)^{-1.5} \quad (3.3)$$

Where E is young's modulus in GPa, F indentation load in N, a and c are half the length of the indentation diagonal and crack length in μm respectively.

3.4.4. Electrical resistance

The electrical resistivity of both monolithic Alumina and Alumina-Ti/Cu composites was determined using the four point probe resistivity measurement in which a 2 mA constant current passes through the two outer probes and measures the voltage through the inner probes which allows the measurement of the samples resistivity using the following empirical equation.

$$\rho = \frac{V}{I}\frac{\pi t}{\left(\frac{sinh\left(\frac{t}{s}\right)}{sinh\left(\frac{t}{2s}\right)}\right)} \quad (3.4)$$

Where V: voltage in volts, I: current in Ampere, t and s are sample thickness and probe spacing respectively.

CHAPTER 4 RESULTS AND DISCUSSION

4.1. Microstructure and Composition

Figure 4.1 shows micrographs obtained by optical microscope (OM). The micrographs presented here correspond to samples sintered at 1300˚C during 3 h, for different contents of Ti and Cu in the composite. It may be observed that the grain growth is greater with increments of titanium and copper content. Samples with 3 wt% Ti and 3 wt% Cu show a microstructure with good distribution and uniform grain size, due to the good thermal conductivity of Ti/Cu that adequately dissipates a portion of the thermal energy generated during sintering; thereby contributing to obtaining the good values of densification showed in the previous section. The opposite occurs with the samples with lower reinforcement content, where non uniform distribution of particles in the microstructures are observed. This situation is due to the significant energy absorption by titanium particles, energy which is consumed by the sample through the grain growth.

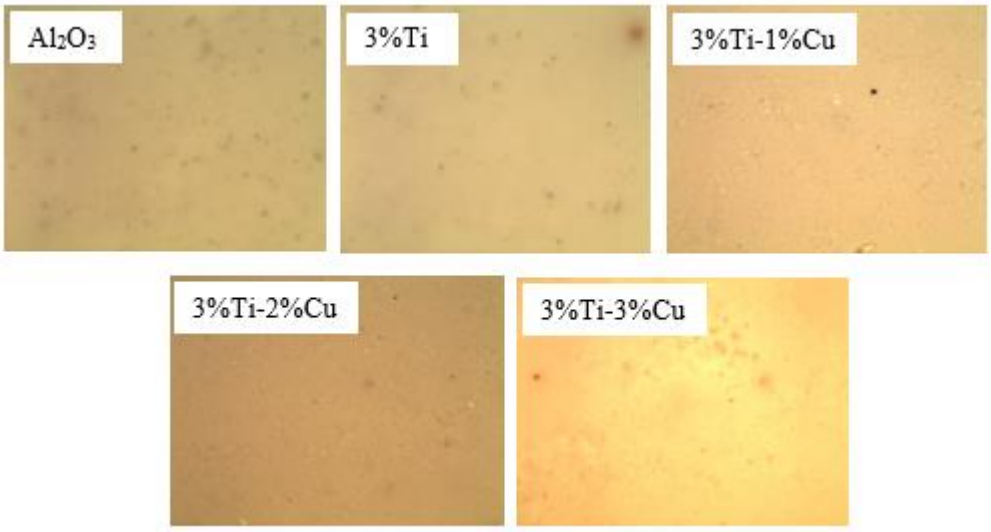

Figure 4.1: Micrographs of the sintered samples at 1300˚C during 3 hours.

Figure 4.2 below represents the x-ray diffraction patterns corresponding to the sintered pure Al_2O_3, 3%Ti, 3%Ti-1%Cu, 3%Ti-2%Cu and 3%Ti-3%Cu composites. Diffractograms indicate Al and O peaks in the pure Al_2O_3 sample. Well distinguishable Al, O, Ti and Cu peaks also can be observed in the Alumina-Ti/Cu composites. No peak relating to new

intermetallic compounds between Alumina and reinforcements can be detected. This confirms no reaction occurs between Al_2O_3 and reinforcement particles and supports the formation of Al_2O_3 composite structures. For the case of the sample with 0 wt% Ti and 0 wt% Cu, obtained spectra indicates the presence of oxygen and aluminum in the sample, feature that corresponds to the composition of the ceramic matrix (Al_2O_3).

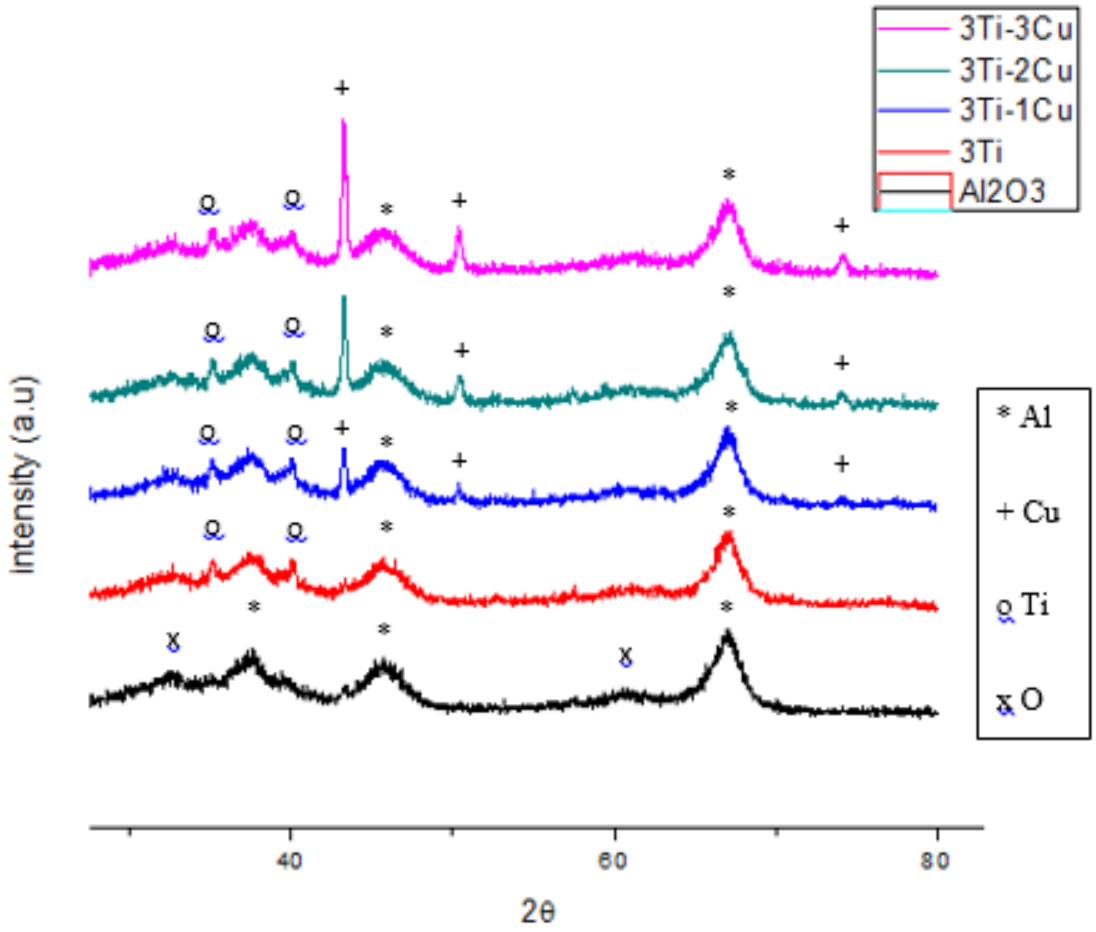

Figure 4.2: X-Ray diffraction patterns of the sintered samples at 1300˚C during 3 hours.

4.2. Density

Results of the relative density measurement of the sintered samples are observed in Figure 4.3. In samples sintered at 1300˚C during 3 h (Figure 4.3 (a)) with contents of 3% Ti and 3% Cu the highest values were obtained, while for greater amounts of Ti there was a downward trend in the density of the composites especially around 1200°C. These results agree with those of granulometry, which show a greater presence of fine particles in the samples with 3% Ti and 3% Cu. This favors compaction of the powders and therefore, a homogeneous grain growth during the sintering. In samples sintered for 2 h with a variation

of the temperature, the positive effect of the inclusion of Ti with respect to monolithic alumina is observed, attaining the highest value of density at 1300˚C. Regarding the samples sintered at 1300˚C for different times, 2 and 3 h (Figure 4.3 (b)), the positive effect of Ti and Cu is similarly observed up to 1300˚C. It can be said that, temperatures of 1200˚C and inclusion of only 3% Ti are not suitable for the consolidation of the samples probably due to a significant grain growth in their microstructures, which also generates a lower elimination of porosity.

Moreover, temperatures of 1100˚C and timing of 2 h sintering are not favorable conditions for consolidating the samples; in this case the distribution is not large enough to achieve the densification of the samples. Therefore, the systems with 3wt% Ti and 3 wt% Cu sintered at 1300˚C during 3 h are the ideal for obtaining better densified samples, since under these conditions almost 99% of the relative density of the samples is reached.

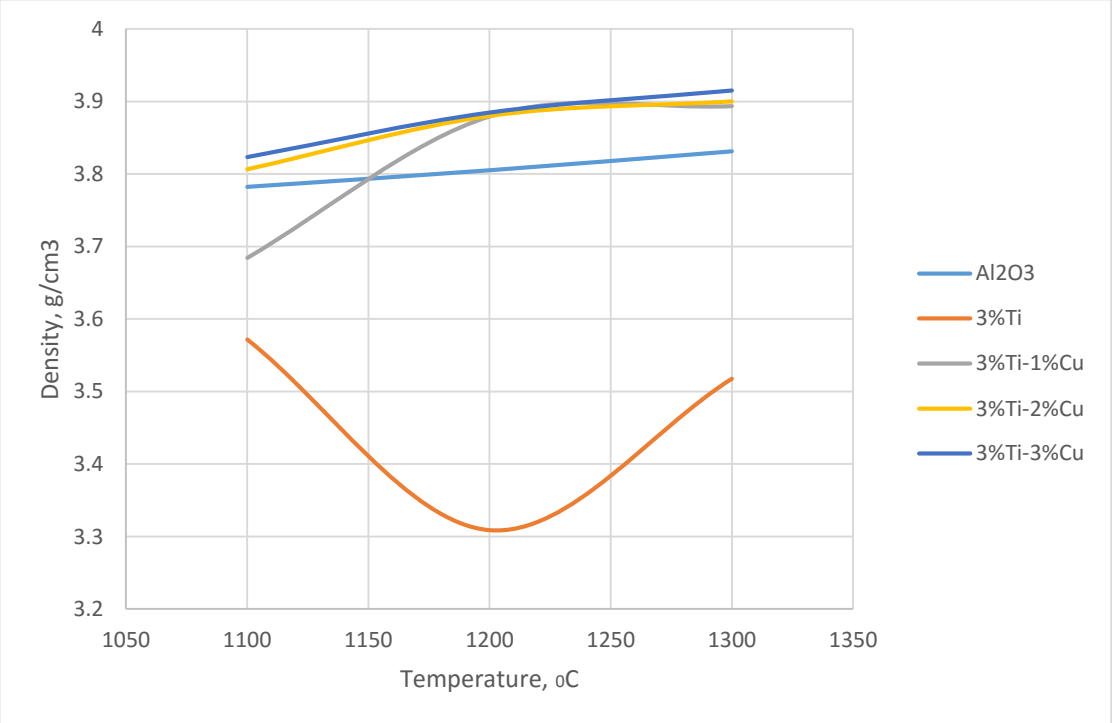

(a)

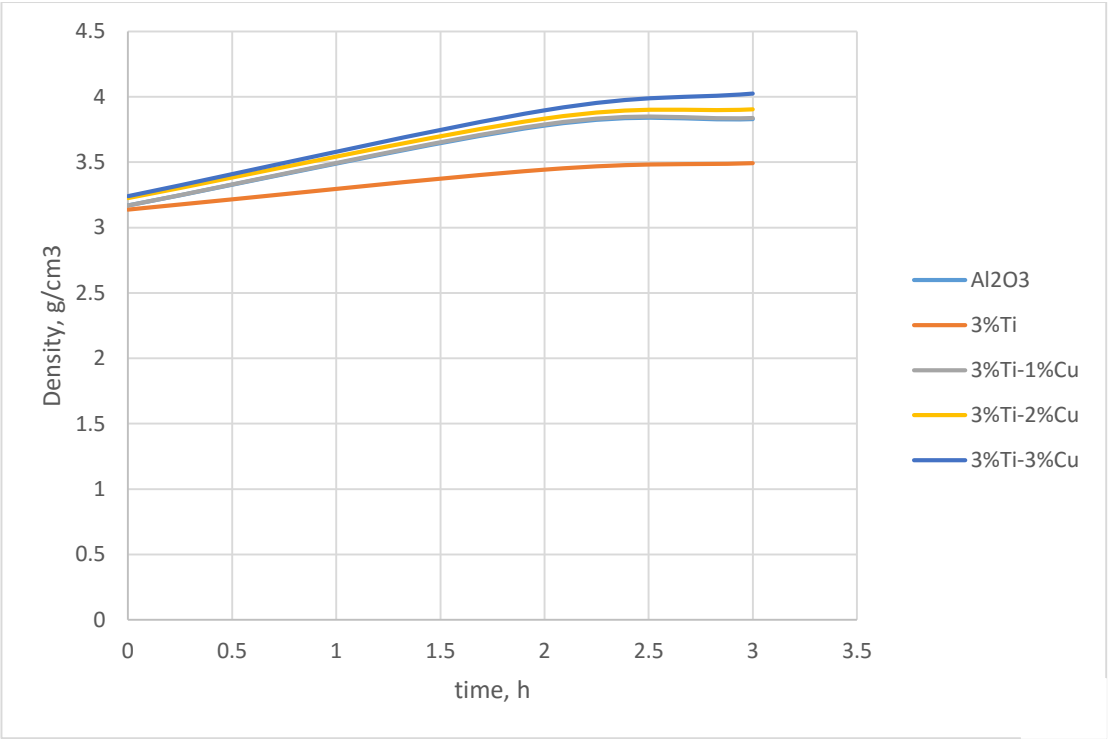

(b)

Figure 4.3: Density of the sintered samples as a function of: (a) sintering temperature and (b) sintering time.

4.3. Mechanical Properties

4.3.1. Hardness

In figure 4.4, two indentations are taken from microhardness testing of samples with 0.0% reinforcement and 3%Ti-3%Cu sintered for 3 hours at 1300˚C are observed. The figure on the left side has a mark obtained in the sample with 0% Ti and Cu, where the growth of a crack in a linear path which apparently spreads easily based on its size can be observed. In the sample with 3% Ti and 3% Cu inclusion (right side), it can be seen that the crack generated at the apex of the mark spreads and stops when it encounters a particle of Ti and Cu, so that it may be concluded that in the Al2O3-Ti/Cu system when a crack grows and hits a particle of Ti or Cu, the ductility and plastic deformation of the metal inhibits the growth of the crack or promotes its search for another propagation path, causing a higher demand of energy for the crack to grow, resulting in an increase in fracture toughness of the material, explaining the strengthening of Al_2O_3 by means of Ti and Cu.

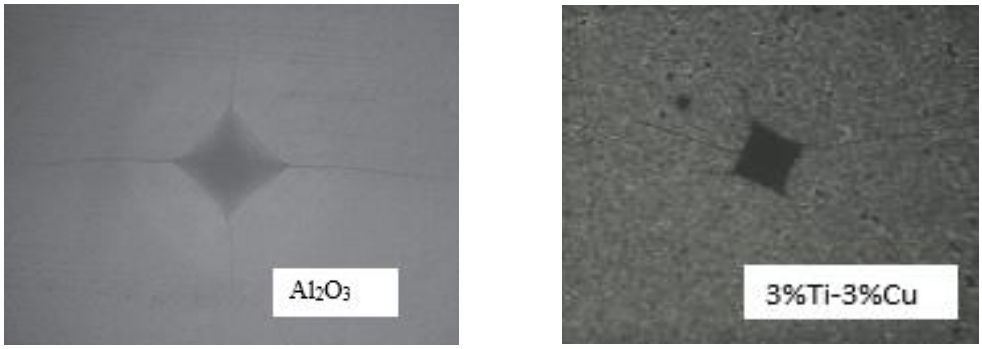

Figure 4.4: Vickers Indentation images of the Al2O3-Ti/Cu composites.

With respect to the hardness results, from Table 4.1 and figure 4.5, it can be seen that for all the systems monolithic Al_2O_3 is the hardest material. All the composite materials present hardness values between 18 and 19 GPa that are less than the almost 21 GPa reported for monolithic Al_2O_3. This is logical because a ceramic material has to be harder than the same ceramic material with the incorporation of ductile phases in its bulk volume.

Table 4.1: Vicker hardness value of the composites at the three sintering temperature ranges, 1100 ºC, 1200 ºC and 1300 ºC.

Matrix Material	Reinforced Metal		HV (GPa)		
	Titanium (wt %)	Copper (wt %)	1100ºC	1200ºC	1300ºC
Al_2O_3	0.0	0.0	21.03	20.97	20.73
	3.0	0.0	19.01	18.98	18.5
	3.0	1.0	18.97	18.95	18.90
	3.0	2.0	18.953	19.10	18.11
	3.0	3.0	18.93	18.6	18.17

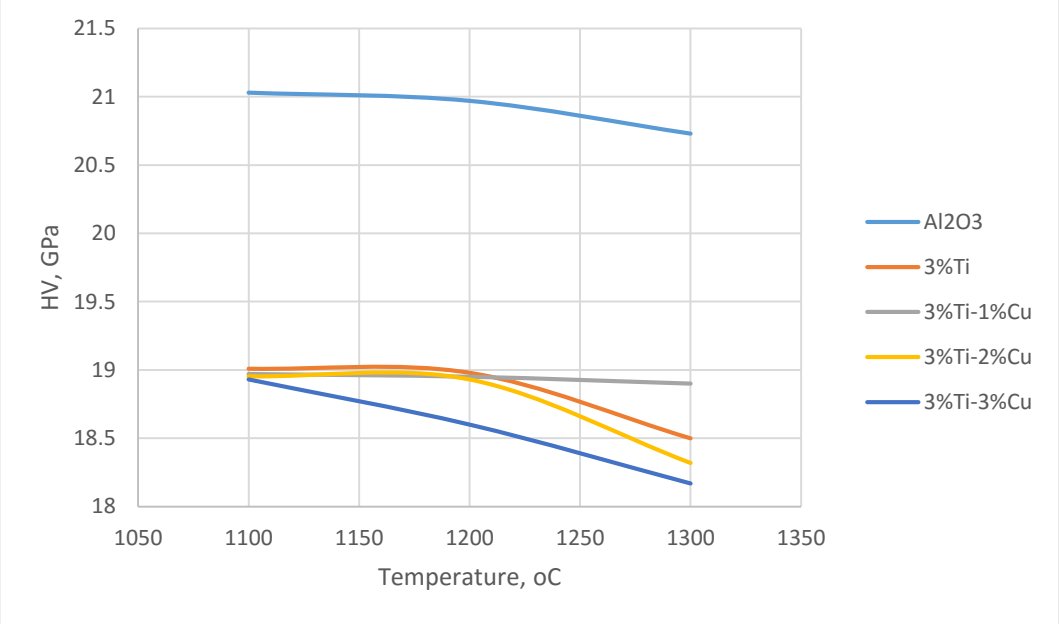

Figure 4.5: Vicker Hardness as a function of temperature for the monolithic alumina and the composites

4.3.2. Fracture toughness

In figure 4.6, the values of fracture toughness as a function of both sintering temperature and time are shown. In the samples with different contents of Ti and Cu and sintered at 1300˚C for 3 h, in relation to fracture toughness positive values up to 150% are achieved compared to the monolithic alumina. These results are consistent with the results of the density measurements and microstructure observations, where it is shown that for the samples with 3%Ti-3%Cu and 3%Ti-2%Cu the controlled grain growth and the homogeneous distribution of Ti and Cu along with the better wettability of Cu with Ti accentuate the obtainment of dense bodies with homogeneous microstructures, conditions that facilitate the strengthening of alumina by these metallic reinforcements.[98] (Figure 4.6(a)) shows the fracture toughness of the composite as a function of temperature and for samples with inclusions of 3%Ti and 3%Cu sintered for 3 h, a considerable effect of Ti and Cu inclusions and of the temperature on fracture toughness is observed due to the 1300˚C at which the highest value of this property is attained. The sintered samples as a function of sintered time (Figure 4.6(b)) show increases in the fracture toughness. Although, these have inferior toughness results compared with those obtained when the temperature was varied.

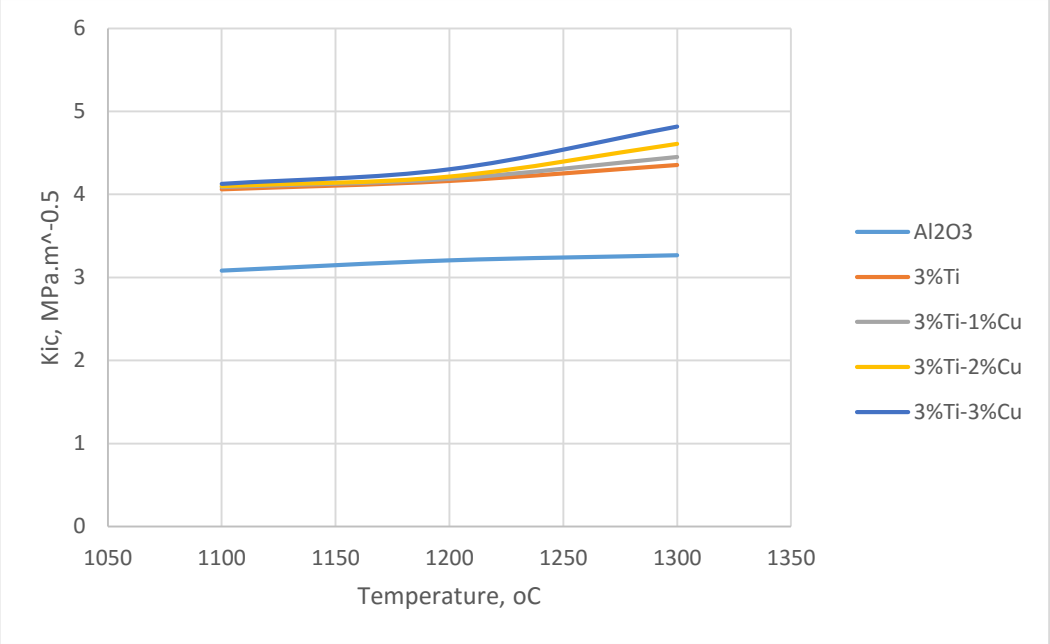

(a)

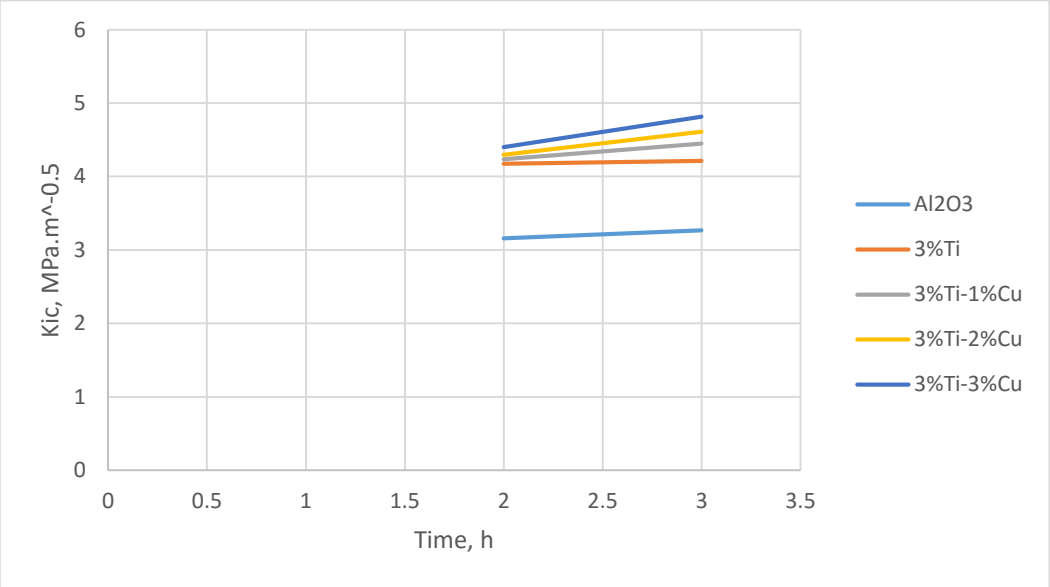

(b)

Figure 4.6: Fracture toughness of the composites Al_2O_3-Ti/Cu as a function of: (a) sintering temperature and (b) sintering time.

4.4. Electrical Resistance

Figure 4.7 displays the electrical resistance results as a function of the Titanium/copper content sintered at 1300 ºC for 3 h in the composites. It can be observed that the electrical resistance reduces with the increments of copper content especially. This can be explained as follows; the results obtained in the composites indicate that the quantity of electrical current under different voltages applied follows a lineal behavior. This allows the determination of the electrical resistance through Ohm's Law, applying a lineal fitting procedure to the experimental data. From the current-voltage experimental data it is estimated the electrical resistance. Comparing these results with the electrical conductivity of the elements constituting the composite it is found that: The alumina has an electrical resistivity $>10^{14}$ Ω-cm [111]. From the data it can be calculated that its electrical conductivity is about $<10^{-14}$ (1/ Ω-cm), this means that it is very difficult for the electricity to pass through it. If the resistance is now computed considering the sample's dimensions, the resistance is $3.4802X10^{13}$ Ω. This means that the incorporation of copper in the ceramic matrix diminishes its electrical resistance in almost 50% for the sample with 30 % Cu.

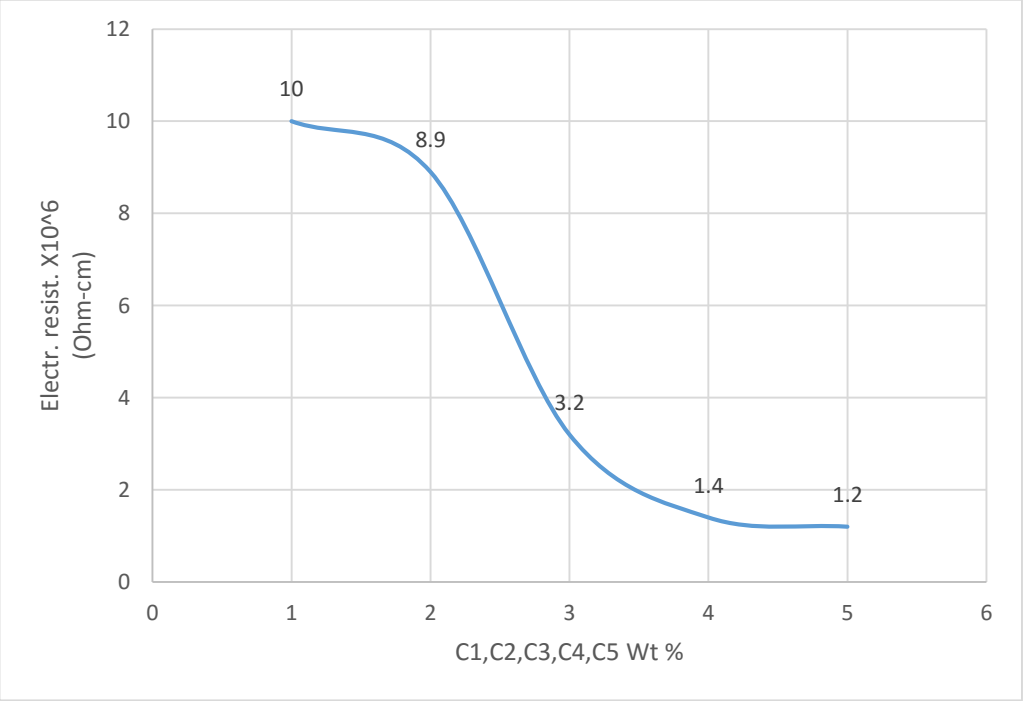

Figure 4.7: Resistivity as a function of composition of reinforcing metals Ti and Cu for the sintering temperature of 1300 ºC for 3h.

CHAPTER 5 CONCLUSIONS AND RECOMMENDATIONS

In this study, alumina was reinforced with Titanium (with a fixed composition) and Copper (with a varying composition) metallic particles in order to observe the effect of those metallic reinforcements on the mechanical properties of the composite and through the processing methodology proposed, dense alumina-based composites strengthened with Ti and Cu metallic particles were obtained.

The fracture toughness of the Al_2O_3 was improved significantly with the reinforcement of the same by means of Ti and Cu nanoparticles homogeneously distributed in the ceramic matrix, by the better wettability of copper with titanium on the matrix. Al_2O_3 reinforced with 3% Ti-3% Cu exhibits a much better density and fracture toughness than the monolithic Alumina and other reinforcement compositions. The strengthening mechanism of Al_2O_3 is due to the crack deflection and crack bridging caused by the presence of homogeneous ductile metallic particles present in intergranular zones of the composite's microstructure. On the other hand, copper and the network that it forms also help to reduce the electrical resistance of the composites.

Therefore, the author recommends reinforcement of alumina ceramics with a precisely controlled composition of titanium and copper could significantly enhance the fracture toughness of Alumina, hence overcomes its limitations in structural applications.

References

[1] J. K. M. F. Daguano, C. Santos et al. (2007) *Properties of ZrO2–Al2O3 Composite as a Function of Isothermal Holding Time*, Int. J. Refract. Metals Hard Mater, 25 374–379.

[2] Y. Wu, Y. Zhang et al. (2001) *Microstructural Development and Mechanical Properties of Self-Reinforced Alumina with CAS Addition*, J. Eur. Ceram. Soc., 21 581–587.

[3] L. Wang, J. Shi, Z. Hua et al. (2001) *The Influence of Addition of WC Particles on Mechanical Properties of Alumina–Matrix Composite*, Mater. Lett, 50 179–182.

[4] H. Miyazaki, Y. Yoshizawa et al. (2004) *Preparation and Mechanical Properties of 10 vol.% Zirconia/Alumina Composite with Fine-Scale Fibrous Microstructure by Extrusion Process*, Mater. Lett, 58 1410–1414.

[5] C. Liu, J. Zhang, J. Sun et al. (2007) *Addition of Al–Ti–B Master Alloys to Improve the Performances of Alumina Matrix Ceramic Materials*, Ceram. Int., 33 1319–1324.

[6] L. Changxia, Z. Jianhua, S. Junlonga et al. (2007) *Addition of Al–Ti–C Master Alloys and Diopside to Improve the Performance of Alumina Matrix Ceramic Materials*, Ceram. Int., 33 1149–1154.

[7] R. Z. Chen and W. H. Tuan (2001) *Toughening Alumina with Silver and Zirconia Inclusions*, J. Eur. Ceram. Soc., 21 2887–2893.

[8] Myer Kutz ed. (2015) Mechanical Engineers' Handbook, Fourth Edition, John Wiley & Sons, Inc.

[9] K. S. W. Sing, D. H. Everett et al. (1985) *Reporting Physisorption Data for Gas/Solid Systems with Special Reference to the Determination of Surface Area and Porosity*. Pure Appl. Chem., **57** (4), pp. 603–619

[10] K. Schwartzwalder and A. V. Somers. (1963) *Patent US 3090034: Method of Making Porous Ceramic Articles*.

[11] A. R. Studart, U. T. Gonzenbach et al. (2006) *Processing Routes to Macroporous Ceramics: A Review*. J. Am. Ceram. Soc., **89** (6), pp. 1771–1789

[12] P. Colombo. (2006) *Conventional and novel processing methods for cellular ceramics*. Phil. Trans. R. Soc. A, **364**, pp. 109–124,

[13] J. Saggio-Woyansky and C. E. Scott. (1992)*Processing of Porous Ceramics*. Am. Ceram. Soc. Bull., **71**, pp. 1674–1682,

[14] F. F. Lange, B. V. Velamakanni et al. (1990) *Method for Processing Metal-Reinforced Ceramic Composites*. J. Am. Ceram. Soc., **73** (2), pp. 388–393,

[15] D. R. Clarke. (1992) *Interpenetrating Phase Composites*. J. Am. Ceram. Soc., **75** (4), pp. 739–759 ,

[16] W. D. Kingery, H. K. Bowen et al. (1976) *Introduction to Ceramics*.Wiley-Interscience, 2 ed. 128-131

[17] N. A. Travitzky and A. Shlayen. (1998) *Microstructure and mechanical properties of Al_2O_3/Cu-O composites fabricated by pressureless infiltration technique*. Mat. Sci. Eng. A, **244** (2), pp. 154–160

[18] R. Brezny, D. J. Green et al. (1989) *Evaluation of Strut Strength in Open-Cell Ceramics*. J. Am. Ceram. Soc., **72** (6), pp. 885–889

[19] D. Brown and D. Green. (1994) *Investigation of Strut Crack Formation in Open Cell Alumina Ceramics*. J. Am. Ceram. Soc., **77** (6), pp. 1467–1472

[20] L. J. Gibson and M. F. Ashby. (1988) *Cellular Solids - Structure and Properties*. Pergamon

[21] K. Konopka, A. Olszowka-Myalska et al. (2003) *Ceramic-metal composites with an interpenetrating network*. Mater. Chem. Phys., **81** (2-3), pp. 329–332

[22] D. J. Cumberland and R. J. Crawford. (1987) *The packing of particles*. Elsevier, Amsterdam, 1 ed.

[23] S. Skirl, M. Hoffman et al. (1998) *Thermal expansion behavior and macrostrain of Al_2O_3/Al with interpenetrating networks*. Acta Mater., **46** (7), pp. 2493–2499

[24] F. R. Cichocki, K. P. Trumble et al. (1998) *Tailored Porosity Gradients via Colloidal Infiltration of Compression-Molded Sponges*. J. Am. Ceram. Soc., **81** (6), pp. 1661–64

[25] F. Stromberger. (1998) *Herstellung von Gradientenwerkstoffen über ortsabhängige Verdichtung polymerer Vorformen*. Diplomarbeit, Technische Universität Darmstadt

[26] A. Neubrand, T. Chung et al. (2002) *Residual stresses in functionally graded plates*. J. Mater. Res., **17** (11), pp. 2912–2920

[27] M. König. (2006) *Herstellung und Charakterisierung eines Kupfer-Aluminiumoxid Verbundwerkstoffs mit Durchdringsgefüge*. Diplomarbeit, Technische Universität Darmstadt

[28] R. Brezny and D. Green. (1990) *The effect of cell size on the mechanical behavior of cellular materials*. Acta Metall. Mater., **38** (12), pp. 2517–2526

[29] A. Mattern. (2004) *Interpenetrierende Metall-Keramik-Verbundwerkstoffe mit isotropen und anisotropen Al_2O_3-Verstärkungen*. Ph.D. thesis, Dissertation Universität Karlsruhe

[30] N. Travitzki and N. Claussen. (1992) *Microstructure and Properties of Metal Infiltrated RBSN Composites*. J. Eur. Ceram. Soc., **9**, pp. 61–65

[31] C. Garcia-Cordovilla, E. Louis et al. (1999) *Overview No. 134 - Pressure infiltration of packed ceramic particulates by liquid metals*. Acta Mater., **47** (18), pp. 4461–4479

[32] K. Prakasan and S. Seshan. (1997) *Electrical conductivity of squeeze cast copper*. J. Mat. Sci. Letters, **16**, pp. 1588–1589

[33] M. Knechtel, H. Prielipp et al. (1994) *Mechanical Properties of Al/Al_2O_3 and Cu/Al_2O_3 Composites with Interpenetrating Networks*. Scr. Metall. Mater., **31** (8), pp. 1085–1090

[34] H. Prielipp, M. Knechtel et al. (1995) *Strength and fracture toughness of aluminum/alumina composites with interpenetrating networks*. Mat. Sci. Eng. A, **197**, pp. 19–30

[35] A. W. Adamson (1982) *Physical Chemistry of Surfaces*, vol. 4th Ed. Wiley-Interscience

[36] P. R. Chidambaram, G. R. Edwards et al. (1994) *Kinetics of Interlayer Formation on Polycrystalline α-Al_2O_3/Copper-Titanium Alloy Interface*. Metall. Mater. Trans. A, **25A**, pp. 2083–2090

[37] P. R. Chidambaram, A. Meier et al (1996) *The nature of interfacial phenomena at copper-titanium/alumina and copper-oxygen/alumina interfaces*. Mat. Sci. Eng. A, **206**, pp. 249–258

[38] I. A. Aksay, C. E. Hoge et al. (1974) *Wetting under Chemical Equilibrium and Nonequilibrium Conditions*. J. Phys. Chem., **78** (12), pp. 1178–1183

[39] N. Eustathopoulos (1998) *Dynamics of Wetting in Reactive Metal/Ceramic Systems*. Acta Mater. **46** (7), pp. 2319–2327

[40] B. Derby, P. Xiao et al. (1998) *Neutron reflection studies of titanium segregation to metal-ceramic interfaces*. Physica B, **248**, pp. 304–309

[41] B. C. Allen and W. D. Kingery (1959) *Surface Tension and Contact Angles in Some Liquid Metal-Solid Ceramic Systems at Elevated Temperatures*. Trans. Metall. Soc. AIME, **215**, pp. 30–37

[42] T. E. O'Brien and A. C. D. Chaklader (1974) *Effect of oxygen on the reaction between copper and sapphire*. J. Am. Ceram. Soc., **57** (8), pp. 329–332

[43] M. Bahraini, L. Weber et al. (2005) *Wetting in infiltration of alumina particle preforms with molten copper*. J. Mat. Sci, **40** (9-10), pp. 2487–2491

[44] F. Delannaz, L. Frozen et al. (1987) *The Wetting of Solids by Molten Metals and its Relation to the Preparation of Metal-Matrix Composites*. J. Mat. Sci, **22** (1), pp. 1–16

[45] A. Meier, M. D. Baldwin et al. (1995) *The effect of large oxygen additions on the wettability and work of adhesion of copper-oxygen alloys on polycrystalline alumina*. Mat. Sci. Eng. A, **196**, pp. 111–117

[46] C. Beraud, M. Courbiere et al. (1989) *Study of copper-alumina bonding*. J. Mat. Sci, **24**, pp. 4545–4554

[47] C. Seager, K. Kokini et al. (2002) *The influence of $CuAlO_2$ on the strength of eutectically bonded Cu/Al_2O_3 interfaces*. Scr. Mater., **46**, pp. 395–400

[48] N. Eustathopoulus and B. Drevet (1994) *Interfacial Bonding, Wettability and Reactivity in Metal-Oxide Systems*. J. Physique, **4** (10), pp. 1865–1881

[49] P. Kritsalis, L. Coudurier et al. (1991) *Contribution To The Study Of Reactive Wetting In The $CuTi/Al_2O_3$ System*. J. Mat. Sci, **26** (12), pp. 3400–3408

[50] V. D. Krstic (1983) *On the fracture of brittle-matrix/ductile-particle composites*. Phil. Mag. A, **48** (5), pp. 695 – 708–695 – 708

[51] T. Emmel, U. Stiefel et al. (2003) *Deformation and Failure in Metallic Materials*, chap. Damage and Failure of Ceramic Metal Composites: Experimental and Numerical Investigations, pp. 203–221. Springer, 1 ed.

[52] A. D. Krawitz and T. M. Holden (1990) *The Measurement Of Residual-Stresses Using Neutron-Diffraction*. MRS Bull., **15** (11), pp. 57–64

[53] P. J. Withers (1995) *Neutron Stain Measurement of Internal Strain in Metal and Ceramic Matrix Composites*. Key Eng. Mater., **108-110**, pp. 291–314

[54] D. Mari, A. D. Krawitz et al. (1996) *Residual stress in WC-Co measured by neutron diffraction*. Mat. Sci. Eng. A, **209** (1-2), pp. 197–205

[55] S. Skirl (1998) *Mechanische Eigenschaften und Thermisches Verhalten von Al_2O_3/Al und Al_2O_3/Ni_3Al Verbundwerkstoffen mit Durchdringungsgefüge*. Fortschritt-Berichte VDI, **5** (536), pp. 1–137

[56] S. Skirl, R. Krause, et al. (2001) *Processing and Mechanical Properties of Al_2O_3/Ni_3Al Composites with Interpenetrating Network Microstructure*. J. Am. Ceram. Soc., **84** (9), pp. 2034–2040

[57] M. Hoffman, S. Skirl et al. (1999) *Thermal Residual Strains and Stresses in Al_2O_3/Al Composites with Interpenetrating Networks*. Acta Mater., **47** (2), pp. 565–577

[58] R. J. Moon, M. Tilbrook et al. (2005) *Al-Al_2O_3 Composites with Interpenetrating Network Structures: Composite Modulus Estimation*. J. Am. Ceram. Soc., **88** (3), pp. 666–674

[59] J. Aboudi (1991) *Mechanics of Composite Materials*. Elsevier Science, 1 ed..

[60] D. Gross and T. Seelig (2001) *Bruchmechanik, mit einer Einführung in die Mikromechanik*. Springer, 3 ed.

[61] W. Voigt. (1889) *Über die Beziehung zwischen den beiden Elastizitätskonstanten isotroper Körper*. Wied. Ann., **38**, pp. 573–587

[62] A. Reuss. (1929) *Berechnung der Fliessgrenze von Mischkristallen auf Grund der Plastizitaetsbedingung fuer Einkristalle* . Zeit. ang. Math. Mech., **9** (1), pp. 49 –58

[63] Z. Hashin and S. Shtrikman (1963) *A Variational Approach to the Theory of the Elastic Behaviour of Multiphase Materials*. J. Mech. Phys. Solid, **11** (2), pp. 127–140

[64] T. W. Hull, D. Clyne (1996) *An Introduction to Composite Materials*. Cambridge University Press, Cambridge, UK, 2 ed.

[65] T. L. Anderson (1995) *Fracture Mechanics: Fundamentals and Applications*. CRC Press, 2 ed.

[66] K. Bowman (2004) *Mechanical Behaviour of Materials*. John Wiley & Sons

[67] B. Lawn (1993) *Fracture of Brittle Solids*. In E. A. Davis and I. M. Ward, eds., *Cambridge Solid State Science Series*. Cambridge University Press, 2 ed.

[68] H. Tada, P. C. Paris et al. (1985) *The Stress Analysis of Cracks Handbook*. Paris Productions, Inc, St. Louis, 2 ed.

[69] A. A. Griffith (1920) *The phenomenon of rupture and flow in solids*. Philosophical Transactions of the Royal Society, **A221**, pp. 163–98

[70] G. R. Irwin (1956) *Onset of Fast Crack Propagation in High Strength Steel and Aluminium Alloys*. Sagamore Research Conference Proceedings, **2**, pp. 289–305

[71] J. Rödel (1993) *Rißüberbrückung in keramischen Werkstoffen*. Fortschritt-Berichte VDI, **5** (331), pp. 1–127

[72] R. Steinbrech, R. Khehans et al. (1983) *Increase Of Crack Resistance During Slow Crack-Growth In Al_2O_3 Bend Specimens*. J. Mater. Sci., **18** (1), pp. 265–270

[73] T. Fett, D. Munz et al. (2000) *Method to Estimate Crack-Tip Toughness from Bending Tests on Prenotched Bars*. J. Am. Ceram. Soc., **83** (2), pp. 421–423

[74] G. R. Irwin (1958) *Handbuch der Physik*, chap. Fracture, pp. 551–594. Springer-Verlag, Berlin

[75] A. Kounga (2003) *Verschiebungsfelder vor und hinter der Rissspitze in verstärkten Keramiken*. Ph.D. thesis, Technische Universität Darmstadt

[76] A. B. Kounga, T. Fett, J. Rödel et al. (2004) *Crack-Tip Toughness Measurements on a Sintered Reaction-Bonded Si_3N_4*. J. Am. Ceram. Soc., **87** (8), pp. 1502–1508

[77] E. Sommer (1981) *Experimental determination of stress intensity factor by COD measurements*. Mech. of Fract., **7**, pp. 331–347

[78] J. Rödel, J. F. Kelly et al. (1990) *In Situ Measurements of Bridged Crack Interfaces in the Scanning Electron Microscope*. J. Am. Ceram. Soc., **73** (11), pp. 3313–3318

[79] G. Pezzotti and O. Sbaizero (2001) *Residual and bridging microstress fields in Al_2O_3/Al interpenetrating network composite evaluated by fluorescence spectroscopy*. Mat. Sci. Eng. A, **303**, pp. 267–272

[80] Z. Burghard, A. Zimmermann et al. (2004) *Crack opening profiles of indentation cracks in normal and anomalous glasses*. Acta Mater., **52** (2), pp. 293–297

[81] M. Hoffman, B. Fiedler et al. (1997) *Fracture behaviour in metal fibre reinforced ceramics*. Acta Mater., **45** (9), pp. 3609–3623

[82] O. Wiener. Abh. (1912) Math-Phys. Kl. Königl. Saechs. Ges., **32**, p. 509

[83] D. K. Hale (1976) *Physical-Properties of Composite-Materials*. J. Mater. Sci., **11** (11), pp. 2105–2141

[84] E. H. Kerner (1956) *The Elastic and Thermo-elastic Properties of Composite Media*. Proceedings of the Physical Society. Section B, **69** (8), p. 808

[85] D. A. G. (1937) Bruggeman. *Berechnung verschiedener physikalischer Konstanten von heterogenen Substanzen. III. Die elastischen Konstanten der quasiisotropen Mischkörper aus isotropen Substanzen*. Ann. Physik, **421** (2), pp. 160–178

[86] P. S. Turner (1946) *Thermal-Expansion Stresses In Reinforced Plastics*. J. Res. Natl Bureau Stand, **37** (4), pp. 239–250

[87] D. Balch, A. Mortensen et al. (1996) *Thermal expansion of metals reinforced with ceramic particles and microcellular foams*. Metall. Mater. Trans. A, **27** (11), pp. 3700–3717

[88] C. Hsieh and W. Tuan (2007) *Thermal expansion behavior of a model ceramic-metal composite*. Mat. Sci. Eng. A, **460-461**, pp. 453–458

[89] ASTME1461-01. *Standard Test Method for Thermal Diffusivity of Solids by the Flash Method*.

[90] Z. Hashin and S. Shtrikman (1962) *A variational approach to the theory of effective magnetic permiability of multiphase materials*. J. Appl. Phys., **33** (10), pp. 3125

[91] K. Lichtenecker (1924) *Der elektrische Leitungswiederstand künstlicher und natürlicher Aggregate*. Phys. Zeit., **8,9**, pp. 169–181,193–204

[92] K. Lichtenecker (1934) *Über die elektrische Leitfähigkeit und andere Körpereigenschaften desselben Typus bei binären Aggregaten*. Zeit. Elektrochem. ang. phys. Chem., **40**, pp. 11–14

[93] Irwin, G.R. (1960). J. Basic Engng ASME. 82, 417.

[94] Griffith A. A. (1921). *The Phenomena of Rupture and Flow in Solids, Phil. Trans*. R. Soc. Lond. pp. 163-198.

[95] ASTM E1820 - 09e1 (2008) *Standard Test Method for Measurement of Fracture Toughness*. Annual Book of ASTM Standards

[96] ASTM C 1327-99, (1999) *Standard Test Method for Fractute Toughness at Room Temperature of Advanced Ceramics*. Annual Book of ASTM Standards, pp. 14-02.

[97] D. Osso, G. Le Caer et al. (1993) *Synthesis of alumina-metal nanocomposites by mechanical alloying*, Journal de Physique **III,** Volume 3

[98] Sergio J. Esparza-Vázquez et al. (2014) *Strengthening of Alumina-Based Ceramics with Titanium Nanoparticles*, Materials Sciences and Applications, 5, 467-474

[99] Wessel, J.K. (2004), *The Handbook of Advanced Materials*. John Wiley & Sons Ltd., New York.

[100] Shackelford, J.F. and Doremus, R.H. (2010) *Ceramic and Glass Materials: Structure, Properties and Processing*. Sp- ringer, Berlin.

[101] Ighodaro, O.L. and Okoli, O.I. (2008) *Fracture Toughness Enhancement for Alumina Systems*: A Review. International Journal of Applied Ceramic Technology, 5, 313-323.

[102] Enrique Rocha-Rangel, David Hernández-Silva et al. (2010) *Alumina-based composites strengthened with titanium and titanium carbide dispersions*, Researchgate,

[103] N. Travitzky, I. Gotman et al. (2003) *Alumina–Ti aluminide interpenetrating composites: microstructure and mechanical properties*, ELSEVIER, Materials Letters 57 3422–3426

[104] E. Rocha-Rangel and J. G. Miranda-Hernández (2010) *Alumina-Copper Composites with High Fracture Toughness and Low Electrical Resistance*, Materials Science Forum Vol. 644 pp 43-46

[105] J. M. Howe (1993) *International Materials Reviews*, Vol. 38 pp. 233.

[106] J. G. Li (1992) J. Amer. Ceram. Soc., Vol. 75 pp. 3118.

[107] Iftikhar Ahmad, Mohammad Islam et al. (2015) *Toughening mechanisms and mechanical properties of graphene nanosheet-reinforced alumina*, Materials and Design

[108] Jerome Lalande, Sven Scheppokat et al. (2002) *Toughening of alumina/zirconia ceramic composites with silver particles*, Journal of the European Ceramic Society

[109] K. Konopka and M. Szafran (2006) *Fabrication of Al2O3–Al composites by infiltration method and their characteristic*, Journal of Materials Processing Technology 175 266–270

[110] Keyvan Piri, Mahdi Shafiee Afarani et al. (2017) *Fabrication of high volume fraction alumina/aluminum composites via reaction sintering route*, Journal of Chemical Technology and Metallurgy, 52, 1

[111] J.F. Shackelford and W. Alexander (2001): Materials Science and Engineering Handbook. CRS Press, Boca Raton Florida